

Ionic Liquids Based on Azolate Anions

**Marcin Smiglak,^[a] C. Corey Hines,^[a] Timothy B. Wilson,^[a] Shailendra Singh,^[b]
Adam S. Vincek,^[b] Kostyantyn Kirichenko,^[b] Alan R. Katritzky,^[b] and
Robin D. Rogers^{*,[a]}**

Abstract: Compartmentalized molecular level design of new energetic materials based on energetic azolate anions allows for the examination of the effects of both cation and anion on the physiochemical properties of ionic liquids. Thirty one novel salts were synthesized by pairing diverse cations (tetraphenylphosphonium, ethyltriphenylphosphonium, *N*-phenyl pyridinium, 1-butyl-3-methylimidazolium, tetramethyl-, tetraethyl-, and tetrabutylammonium) with azolate anions (5-nitrobenzimidazole, 5-nitrobenzotriazole, 3,5-dinitro-1,2,4-triazolate, 2,4-

dinitroimidazole, 4-nitro-1,2,3-triazolate, 4,5-dinitroimidazole, 4,5-dicyanoimidazole, 4-nitroimidazole, and tetrazolate). These salts have been characterized by DSC, TGA, and single crystal X-ray crystallography. The azolates in general are surprisingly stable in the systems explored. Ionic liquids were obtained with all combinations of the 1-butyl-3-methylimidazoli-

um cation and the heterocyclic azolate anions studied, and with several combinations of tetraethyl- or tetrabutylammonium cations and the azolate anions. Favorable structure–property relationships were most often achieved when changing from 4- and 4,5-disubstituted anions to 3,5- and 2,4-disubstituted anions. The most promising anion for use in energetic ionic liquids of those studied here, was 3,5-dinitro-1,2,4-triazolate, based on its contributions to the entire set of target properties.

Keywords: azolates • energetic materials • ion exchange • ionic liquids • organic anions

Introduction

Ionic liquids (ILs), due to their structural composition, form a unique architectural platform on which, at least potentially, the properties of cation and/or anion components can be independently modified.^[1] This allows for tunability in the design of new functional materials, while retaining the core features of the IL state of matter. Assessable properties of ILs such as high ion content, liquidity over a wide temperature range, low viscosity, limited volatility, and high ionic conductivity, have obvious and immediate advantages over traditional solvents. Over the last several years these proper-

ties have proven to be important drivers^[2–7] supporting numerous advances beyond initial investigations of ILs as liquid electrolytes.^[8] Current topics of interest include electrochemistry,^[9–12] separation science,^[13–18] chemical synthesis,^[3,5,6,19–24] catalysis,^[5,6,21,25,26] and many others. The preparation of ILs, their properties, and application in various fields of chemistry have been recently extensively reviewed.^[24,27–30]

It is now believed that it is possible to form any specific IL composition depending on the user's needs, and that the desired chemical and physical properties can be realized in a single salt, by proper selection of the component ions, or in mixtures of component ions. These IL design approaches can be used as a platform strategy to deliver different functional attributes, in the corresponding cationic and anionic components of the ILs (Figure 1). Thus, essentially IL versatility arises from the inherent modularity in ILs themselves, where a suitable combination of ions can be developed to solve each given problem, by providing the exact combination of physical and chemical properties needed.

Additionally, the growing social pressure for new green technologies, and the promise of ILs to deliver such, has led to high academic and industrial interest in IL technologies and applications.^[2–8,27,29] These include utilization of ILs for

[a] Dr. M. Smiglak, C. C. Hines, T. B. Wilson, Prof. R. D. Rogers
Department of Chemistry and Center for Green Manufacturing
The University of Alabama, Box 870336
Tuscaloosa, AL 35467-0338 (USA)
Fax: (+1)205-348-0823
E-mail: RDRogers@bama.ua.edu

[b] Dr. S. Singh, Dr. A. S. Vincek, Dr. K. Kirichenko,
Prof. A. R. Katritzky
Center for Heterocyclic Compounds, University of Florida
Department of Chemistry, Gainesville, FL 32611-7200 (USA)

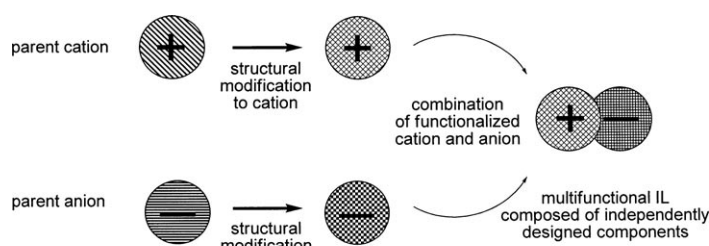


Figure 1. Cations and anions may incorporate functionality independently into ILs.

the processing of cellulose,^[31] biphasic processes (e.g., BASF's BASIL process),^[32] photovoltaics,^[33] fuel cell electrolytes,^[34–36] thermal fluids,^[37,38] lubricants,^[39,40] and many new materials applications. One such new application is in the field of energetic materials.^[41] Our interest in functionalized heterocycles in this context comes from i) the ongoing study of the formation of ILs containing energetic components, in which heterocycles furnish either: the cation, the anion, or both, and ii) investigation of the influence of heterocycle substitution patterns on the ability of these materials to form ILs.^[42–47]

Safety issues and environmental concerns have produced an outstanding need for new, safe, high performance energetic materials.^[48] Ideally, materials development has focused upon designing products that excluded the use of hazardous and potentially toxic compounds such as hydrazine, metals, halides, and perchlorates. Currently used energetic materials often inherit the problematic issues associated with their physical and chemical properties (e.g., polymorphism, which may influence the sensitivity of the material; high melting points, and the need to use plasticizers for the processing of materials for energetic applications).^[49] Such issues present limitations in the safe storage and handling of these energetic materials.

There are a number of benefits of having liquid rather than solid energetic materials; however, in most cases, energetic liquids tend to have high vapor pressures, which can result in loss of material, composition changes, and/or increased hazards. Thus, endowing energetic materials with IL behavior rather than merely the liquid state is an attractive venture.^[41]

Energetic ILs are potentially new materials with thermodynamically high energy yields on combustion^[50] that are “ionic liquids” in physical form. By exploiting the unique attributes of the IL state of matter (especially broad liquidus ranges), many of the problems previously mentioned with energetic materials may be overcome. Polymorphs would not be possible as in the solid state, and additionally, sensitivity of the material to shock would be suppressed.^[51] Due to the negligible vapor pressure, safety issues related to transportation, handling, and processing become favorable from production to end-use.

ILs containing azolate anions (imidazolate, triazolate, tetrazolate, benzimidazolate, or benzotriazolate) have received

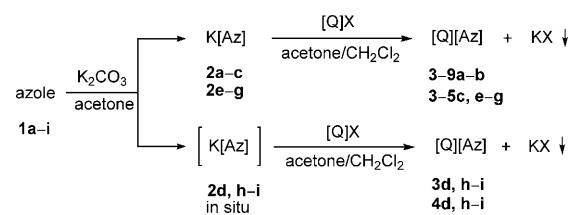
much less attention than those containing azolium cations, although more results are now starting to appear. A small number of tetraalkylammonium and tetraalkylphosphonium 1,2,4-triazolates and imidazolates have been described as solvents and highly active catalysts for oligomerization of isocyanates in the patent literature.^[52] Stearcey et al. has reported tetrabutylammonium 4-nitroimidazolate,^[53] a higher melting salt, as an intermediate for the synthesis of *N*-alkyl-4-nitroimidazoles. Ohno et al. described the preparation and electrochemical properties of two ILs, 1-ethyl-3-methylimidazolium tetrazolate and triazolate, which were prepared via reaction of imidazolium hydroxide (generated by anion-exchange from the halide) with the corresponding azole.^[54,55] Moreover, Shreeve and co-workers^[56–59] have reported a wide range of energetic azolium azolate salts based on 4,5-dinitroimidazolate and 3,5-dinitro-1,2,4-triazolate anions with melting points approaching the definition of ionic liquids and with high heats of formation. Recently, Liotta et al.^[60] disclosed, in a patent application, a method for the formation of a novel energetic ionic liquid comprised of a tetrazolate anion and a tetrazolium cation. Klapötke et al.^[61] recently reported on the preparation of the energetic alkali metal salts based on the 5-nitrotetrazolate anion. Authors speculated on use of those compounds as an environmentally friendly alternative to lead(II) azide; commonly used, highly toxic primary explosive in initiating devices.

Over the past few years, our group has also investigated the possible use of azolate anions for the preparation of low melting energetic ionic liquids.^[62] From our perspective, the use of such anions to form energetic salts, specifically with the addition of energetic substituents (nitro or cyano groups) to enhance their energetic capabilities is a very interesting approach. We recently reported a series of ILs containing substituted imidazolate, triazolate, tetrazolate anions paired with different cations and showed that salts of a wide range of heterocyclic azolate anions with 1-butyl-3-methylimidazolium cation gave several examples of room temperature ionic liquids.^[43,62] In general it was found that these organic anion-based salts allowed for a similar degree of facile functionalization, due to structural similarity with the well-studied azolium cations.^[57,63,64]

To extend the scope of ILs, greater availability of organic anions providing the same, or similar, architectural flexibility as the commonly used organic cations (e.g., substituted imidazolium cations) needs to be achieved. Parallel to this, improvements in the basic understanding of the key physical and chemical properties of complex azolate-based ionic liquids must be obtained.

Here, we report the synthesis and characterization of 31 novel organic salts based on tetraalkylammonium, 1,3-dialkylimidazolium, pyridinium, and phosphonium cations combined with energetically-substituted tetrazolate, triazolate, imidazolate, benzimidazolate, and benzotriazolate anions (Figure 2). Many of the neutral azoles used as precursors to the azolate anions, are energetic heterocyclic compounds which have been previously extensively studied as potential propellants and/or explosives.^[65,66] The ability to

readily form azolate-based IL examples with enhanced stability relative to the starting heterocycles (controlled melting points, higher thermal decomposition temperatures, reduced volatility, etc.), and the generic observation that IL materials can be formed from a wide range of flat heterocyclic anions by modification or selection of the appropriate ions, sets out principles by which ILs containing this class of anions can be developed and exploited.



Scheme 1. Synthetic routes utilized to form azolate-based salts.

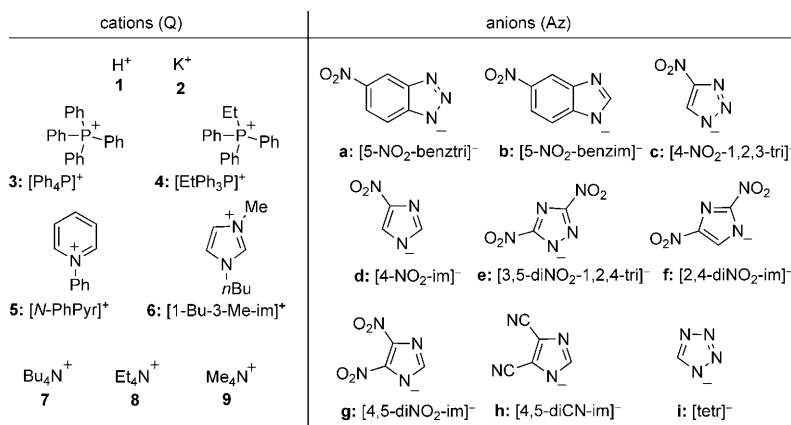


Figure 2. Cation and anion combinations explored in this work.

Results and Discussion

A diverse set of organic salts, combinations of cations **3–9** (**Q**) and anions **a–i** (**Az**) (Figure 2), were prepared by metathesis chemistry. Corresponding potassium azolates were combined with the corresponding ammonium or phosphonium halides in a solvent mixture of acetone/dichloromethane 1:1, at 20–25 °C (Scheme 1). The cations included tetraphenylphosphonium **3** ($[\text{Ph}_4\text{P}]^+$), ethyltriphenylphosphonium ($[\text{EtPh}_3\text{P}]^+$) **4**, *N*-phenylpyridinium **5** ($[\text{N-PhPyr}]^+$), 1-butyl-3-methylimidazolium **6** ($[\text{1-Bu-3-Me-im}]^+$) (commonly known as $[\text{C}_4\text{mim}]^+$), tetrabutylammonium **7** ($[\text{Bu}_4\text{N}]^+$), tetraethylammonium **8** ($[\text{Et}_4\text{N}]^+$), and tetramethylammonium **9** ($[\text{Me}_4\text{N}]^+$). The anions included 5-nitrobenzotriazolate **a** ($[\text{5-NO}_2\text{-benztri}]^-$), 5-nitrobenzimidazolate **b** ($[\text{5-NO}_2\text{-benzim}]^-$), 4-nitro-1,2,3-triazolate **c** ($[\text{4-NO}_2\text{-1,2,3-tri}]^-$), 4-nitroimidazolate **d** ($[\text{4-NO}_2\text{-im}]^-$), 3,5-dinitro-1,2,4-triazolate **e** ($[\text{3,5-diNO}_2\text{-1,2,4-tri}]^-$), 2,4-dinitroimidazolate **f** ($[\text{2,4-diNO}_2\text{-im}]^-$), 4,5-dinitroimidazolate **g** ($[\text{4,5-diNO}_2\text{-im}]^-$), 4,5-dicyanoimidazolate **h** ($[\text{4,5-diCN-im}]^-$), and tetratozolate **i** ($[\text{tetr}]^-$).

Potassium azolate salts **2a–c**, **e–g** were prepared by treatment of the corresponding azoles **1a–c**, **e–g** with potassium carbonate in acetone. The potassium azolates **2a–c**, **e–g** were reacted with equimolar amounts of halide salts of **3–9** and precipitated KX was filtered. Isolation of the corresponding azolates **3–9a–b** and **3–5c**, **3–5e–g** was performed, in vacuo from the filtrate, in 88–99% yield. Difficult isolation of pure salts **2d**, **h**, and **i** was bypassed, by in situ gener-

ation with K_2CO_3 , for the synthesis of 4-nitroimidazolates **3–4d**, 4,5-dicyanoimidazolates **3–4h**, and tetrazolates **3–4i**. Azoles **1d**, **h–i** were treated with in situ potassium carbonate and halide salts of **3–4** to give good yields of salts **3–4d**, **h–i** after removal of inorganic salts.

Structures of salts **3–9a–b** and **3–5c–i** were supported by ^1H and ^{13}C NMR spectra, and elemental analyses (see Experimental Section). As presented in the Experimental Section, the crude products were mostly isolated as hydrates, supported

by the elemental analyses. Most of the samples were recrystallized from alcohol prior to further thermal and crystallographic analysis. Eighteen of the salts were characterized by single crystal diffraction techniques. The family of $[\text{Ph}_4\text{P}]^+$ salts are discussed in detail throughout the text, however cif files for all 19 salts can be obtained from The Cambridge Crystallographic Data Centre.

Thermal characterization

The thermal behavior of the salts was characterized by differential scanning calorimetry (DSC; see Table 1), and thermogravimetric analysis (TGA; see Table 2). The salts varied from high melting solids (**3a**, **c–i**; **4a**, **e**; **5c**, **e–g**; **8b**; **9a**, **b**) to ILs (m.p. <100 °C; **3b**; **4b–d**, **f–i**; **5a**; **6a**, **b**; **7a**, **b**; **8a**).

DSC analyses: All crystalline salts displayed a sharp melting transition on heating, and crystallized on cooling from the melt. However, several of the lower melting salts crystallized very slowly on cooling from the melt and the melting transitions were poorly defined in the DSC, commonly having a characteristic broad transition with a strong “leading edge”. In contrast, the crystallization peaks during heating cycles were exceptionally sharp for those examples. This behavior has been observed for other IL-forming salts.^[67] The melting points and glass transitions for **3a–i** to **9a–i** are shown in (Table 1).

A few of the salts analyzed gave irreversible thermal transitions observable only during the first DSC heating cycle.

Table 1. Melting point and glass transitions [°C] for **3a–i** to **9a–i**.^[a]

| | | [Ph ₄ P] ⁺ (3) m.p. [°C] | [EtPh ₃ P] ⁺ (4) m.p. [°C] | [N-PhPyr] ⁺ (5) m.p. [°C] | [1-Bu-3-Me-im] ⁺ (6) m.p. [°C] | [Bu ₄ N] ⁺ (7) m.p. [°C] | [Et ₄ N] ⁺ (8) m.p. [°C] | [Me ₄ N] ⁺ (9) m.p. [°C] |
|-------------------------------------------------|-----|------------------------------------------------------------|--------------------------------------------------------------|--------------------------------------------------|-------------------------------------------------------|------------------------------------------------------------|------------------------------------------------------------|------------------------------------------------------------|
| [5-NO ₂ -benztri] [−] | (a) | 145 ^[b,c] | 131 ^[b] | 75 ^[b] | −41 ^[d] | 60 ^[b,c] | 64 ^[b] | 192 (at <i>T</i> _{decomp}) |
| [5-NO ₂ -benzim] [−] | (b) | 55 ^[b] | 88 ^[b] | — | −34 ^[d] | 81 ^[b] | 101 ^[b,c] | 119 ^[b,c] |
| [4-NO ₂ -1,2,3-tri] [−] | (c) | 155 | 97 ^[b] | 135 ^[b,c] | −73 ^[d,e] | 87 ^[e] | 82 ^[e] | 157 ^[e] |
| [4-NO ₂ -im] [−] | (d) | 171 | 100 ^[c] | — | −63 ^[d,e] | 106 ^[e] | 124 ^[e] | 185 ^[e] (at <i>T</i> _{decomp}) |
| [3,5-diNO ₂ -1,2,4-tri] [−] | (e) | 171 | 127 ^[b] | 167 | 33 ^[e] | 139 ^[e] | 114 ^[e] | 214 ^[e] (at <i>T</i> _{decomp}) |
| [2,4-diNO ₂ -im] [−] | (f) | 195 | 70 ^[b] | 143 | −53 ^[d,e] | 81 ^[e] | 86 ^[e] | 181 ^[e] |
| [4,5-diNO ₂ -im] [−] | (g) | 145 ^[b,c] | 97 ^[b] | 140 | −64 ^[d,e] | 85 ^[e] | 84 ^[e] | 215 ^[e] (at <i>T</i> _{decomp}) |
| [4,5-diCN-im] [−] | (h) | 149 ^[c] | −29 ^[d] | — | −74 ^[d,e] | 79 ^[e] | 118 ^[e] | 197 ^[e] (at <i>T</i> _{decomp}) |
| [tetr] [−] | (i) | 290 (at <i>T</i> _{decomp}) | 51 ^[b,c] | — | −82 ^[d,e] | −66 ^[d,e] | 114 ^[e] | 216 ^[e] (at <i>T</i> _{decomp}) |

[a] Melting (m.p.) or glass transition (*T*_g) points were measured from the transition onset temperature and determined by DSC from the second heating cycle at 5 °C min^{−1}, after initially melting and then cooling samples to −100 °C unless otherwise indicated. Salts meeting the definition of ionic liquids (m.p. < 100 °C) are in **bold**. [b] Glass transition temperatures (°C) of supercooled liquids (i) with consecutive crystallization and melting on heating; **3a**, 30; **3b**, 22; **3g**, 15; **4a**, 9; **4c**, −8; **4e**, −5; **5c**, −19; **7a**, −32; **7b**, −21; **8a**, −38; **8b**, −30; **9b**, 22 (°C); (ii) with no crystallization and melting under experimental conditions: **4b**, 15; **4f**, −4; **4g**, −11; **4i**, 2; **5a**, 7 (°C). [c] Irreversible transition, from first heating; **3a**, 133; **3g**, 151; **3h**, 159; **4d**, 71, **4h**, 159; **4i**, 94; **5c**, 114; **7a**, 92; **8b**, 37; **9b**, 66 (°C). [d] Glass transitions on heating. [e] Ref. [62].

We speculate that in the cases of **4h**, **4i**, **5c**, **7a**, **8b**, and **9b** the observed transitions were related to the thermal transition of the hydrate form of the salt. The presence of the hydrate in these samples was supported additionally by the observation in TGA analysis of a first small decomposition step (~100–120 °C) in the original samples, prior to major decomposition. For samples **3a**, **3g**, **3h**, and **4d** that showed an irreversible thermal transition during the first heating cycle but no presence of a decomposition step in the TGA experiment that could be ascribed to evaporation of water, possible formation of a thermally more stable polymorph of the salt could not be ruled out.

The tetraphenylphosphonium **3** salts exhibited high melting points between 145–290 °C, with the exception of [Ph₄P][5-NO₂-benzim] **3b**. The less symmetric [EtPh₃P]⁺ **4** salts showed significantly lower melting points. The melting points between phosphonium cations **3** and **4** with the anions [3,5-diNO₂-1,2,4-tri] **e**, [4-NO₂-1,2,3-tri] **c**, and [4-NO₂-im] **d** differed by nearly 50 °C. The large decrease in melting points was observed without any significant change in the thermal stability of the analogous compounds and a widened liquidus range was noted. These are the first reported examples of phosphonium-based azolate ILs.

All but one of the investigated [N-PhPyr]⁺ **5** salts were solids, and in most cases melting points were in a range between those of [Ph₄P]⁺ and [EtPh₃P]⁺ salts (see Table 1). Of the investigated pyridinium salts, only **5a** exhibited a melting point < 100 °C.

Consistent with previous observations,^[62] salts of cation **6**, in particular [1-Bu-3-Me-im][5-NO₂-benztri] **6a** and [1-Bu-3-Me-im][5-NO₂-benzim] **6b**, exhibited the lowest glass transition temperatures of −41 and −34 °C, respectively. As expected, the freezing and melting transitions were suppressed, due to the lower symmetry, charge diffuse, [1-Bu-3-Me-im] cation. In contrast, almost all of the [Ph₄P]⁺ salts melted above 100 °C, except for **3b**. Salts **3c–f**, **h–i** exhibited simple thermal behavior, with broad melting and sharp crystallization, independent of the sample's thermal history. After forming supercooled liquids, though an initial melting

and cooling cycle, **3a** and **3g** crystallized on heating prior to the expected melting point transition. Thermal analysis of the first DSC cycle, indicated **3a** and **3g**, regardless of their initial melting point temperatures (133 and 151 °C, respectively), remained liquid until cooled to 30 and 15 °C, respectively. The observed phase transitions were recognized as glass transitions, possibly affected by change in the mobility of the cations in the supercooled phase.

A large number of salts exhibited similar supercooled liquid characteristics under the same conditions during DSC analysis; representative examples **3a**, **4a**, **4f**, and **4g** are shown in Figure 3. Observable close-to-ambient glass transition temperatures on cooling and heating are related to thermally dependent mobility of transitions followed by crystallization and consecutive melting on heating, were recorded for **3a,b,g**, **4a,c,e**, **5c**, **7a,b**, **8a,b**, and **9b**, or, followed by no crystallization/melt at all, were recorded for **4b,f,g,i**, and **5a**.

The effect of the anion structure and its composition was examined in relation to the melting point change. It was noted that the triazole [4-NO₂-1,2,3-tri][−] salts (**3,4,6–9c**) melt at lower temperatures than the imidazole [4-NO₂-im][−] salts (**3,4,6–9d**) suggesting that the presence of an additional nitrogen atom in the former heterocycle plays an important role in melting point variation (Table 1). Moreover, the salts based on [4-NO₂-1,2,3-tri][−], not only exhibit lower melting points, they generally possess higher thermal stabilities than analogous [4-NO₂-im][−] salts (Table 1, row **c** and **d**). Structural differences between the [4-NO₂-im][−] and [4-NO₂-1,2,3-tri][−] anions, that is, replacement of the C2 atom with a nitrogen atom in [4-NO₂-1,2,3-tri][−], may increase the number of available hydrogen-bond acceptor sites in the anion. Since there are more hydrogen-bonding active sites, the overall electron density around the ring would be more delocalized, thus the interactions with the heterocyclic ring would be weaker, presumably lowering the lattice energy and the melting point of formed salts. From an energetic materials applications point of view, utilization of compounds based on triazolate anions, instead of the imidazolate anions also

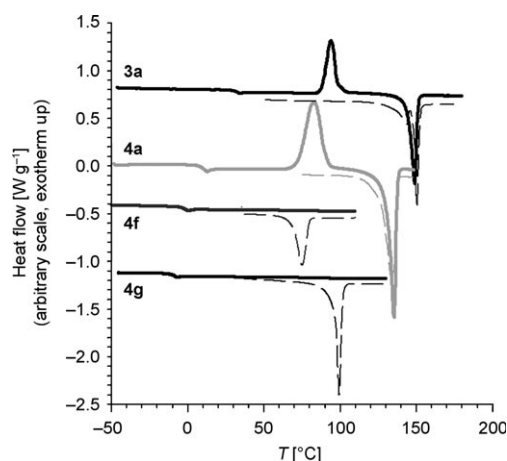


Figure 3. Examples of supercooled liquid behavior. The first heating cycle is shown as a dashed line and the second heating cycle is shown as a solid line. Samples **3a** and **4a** after initial melting did not crystallize on cooling, but formed supercooled phases, which upon the second heating cycle underwent a consecutive glass transition, crystallization, and melting. Samples **4f** and **4g** after initial melting did not crystallize, but formed supercooled phases, which upon heating exhibited glass transitions with no further thermal phase transitions.

gives the additional advantage that both oxygen balance (amount of oxygen required vs present needed for complete combustion of the compound) and nitrogen content (amount of nitrogen in the molecule expressed in value of mass %) of the product are greatly improved. For example, energetic applications that require low combustion temperatures (e.g., gas generators for airbags or fire extinguishing systems) strongly benefit from reduced carbon content and increased nitrogen content.

The similar melting points of $[4,5\text{-diNO}_2\text{-im}]^-$ and $[4,5\text{-diCN-im}]^-$ anion-based salts suggest that melting point may be influenced more by spatial contributions of substituents in the C4 and C5 positions, rather than by the electronic character as shown in the solid-state where similar packing efficiencies and hydrogen bonding are observed. We found

that the introduction of more oxygen-rich NO_2 groups on the anion ring, such as in $[2,4\text{-diNO}_2\text{-im}]^-$ and $[4,5\text{-diNO}_2\text{-im}]^-$, compared to $[4\text{-NO}_2\text{-im}]^-$, did not significantly influence the melting points of the salts, with a maximum difference of 40°C for **8d** and **8g**. These observations, if generally applicable, are beneficial for maintaining IL behavior while introducing additional energetic functionalities into the structure of the azolate anion ring.

TGA analyses: Thermal data for **3–9a–i** are shown in (Table 2). All of the salts are stable to greater than 150°C with the exception of $[\text{Me}_4\text{N}][5\text{-NO}_2\text{-benzim}]^-$ **9b**, for which the $T_{5\% \text{ decomp}}$ temperature was recorded at $\sim 141^\circ\text{C}$. It was noted that the stabilities of the $[\text{Ph}_4\text{P}]^+$ salts (decomposition temperatures ranging from $223\text{--}368^\circ\text{C}$) were markedly higher than those of the $[\text{EtPh}_3\text{P}]^+$ salts (ranging from $219\text{--}291^\circ\text{C}$). Future utilization of phosphonium salts appears promising for high temperature applications.

Few of the investigated salts exhibited simple thermal decomposition behavior. The tetraalkylammonium salts did show single step decomposition with an 85 % mass loss over a 70°C window, except for $[\text{Me}_4\text{N}][5\text{-NO}_2\text{-benzim}]^-$ **9b**, which exhibited a less defined decomposition thermogram. In most other cases, the samples decomposed in two consecutive steps. The first decomposition step for most of the $[\text{Ph}_4\text{P}]^+$ salts (except for samples **3b** and **3g** which exhibited single-step decomposition) was found in the range of $223\text{--}368^\circ\text{C}$ and the second decomposition step in the range of $\sim 490\text{--}528^\circ\text{C}$, with sample masses remaining after the first decomposition step in the range of 12 to 35 % (Figure 4, example **3h**). A two-step decomposition also occurred for $[\text{EtPh}_3\text{P}]^+$ salts, with the first decomposition in the range $219\text{--}291^\circ\text{C}$, and the second decomposition step in a much narrower range of $471\text{--}500^\circ\text{C}$, with sample masses remaining after the first decomposition step in the range of $\sim 9\text{--}35\%$ (Figure 4, example **4a**). (Multiple decomposition steps for tetraalkylphosphonium-based salts have been previously reported in the literature.^[68])

Table 2. Thermal stabilities $^\circ\text{C}$ for **3a–i** to **9a–i**.^[a]

| | | $[\text{Ph}_4\text{P}]^+$ (3) | $[\text{EtPh}_3\text{P}]^+$ (4) | $[\text{N-PhPyr}]^+$ (5) | $[\text{1-Bu-3-Me-im}]^+$ (6) | $[\text{Bu}_4\text{N}]^+$ (7) | $[\text{Et}_4\text{N}]^+$ (8) | $[\text{Me}_4\text{N}]^+$ (9) |
|------------------------------------------|-----|----------------------------------------------------------------------|----------------------------------------------------------------------|----------------------------------------------------------------------|----------------------------------------------------------------------|----------------------------------------------------------------------|----------------------------------------------------------------------|----------------------------------------------------------------------|
| | | $T_{5\% \text{ decomp}}$ (T_{decomp}) $^\circ\text{C}$ | $T_{5\% \text{ decomp}}$ (T_{decomp}) $^\circ\text{C}$ | $T_{5\% \text{ decomp}}$ (T_{decomp}) $^\circ\text{C}$ | $T_{5\% \text{ decomp}}$ (T_{decomp}) $^\circ\text{C}$ | $T_{5\% \text{ decomp}}$ (T_{decomp}) $^\circ\text{C}$ | $T_{5\% \text{ decomp}}$ (T_{decomp}) $^\circ\text{C}$ | $T_{5\% \text{ decomp}}$ (T_{decomp}) $^\circ\text{C}$ |
| $[5\text{-NO}_2\text{-benztri}]^-$ | (a) | 273 (305) ^[b] | 247 (279) ^[b] | 158 (162) ^[b] | 186 (209) ^[b] | 174 (202) | 178 (205) | 177 (197) |
| $[5\text{-NO}_2\text{-benzim}]^-$ | (b) | 223 (256) | 220 (270) ^[b] | – | 177 (189) ^[b] | 169 (194) | 169 (193) | 141 (161) ^[b] |
| $[4\text{-NO}_2\text{-1,2,3-tri}]^-$ | (c) | 273 (308) ^[b] | 241 (284) ^[b] | 192 (201) ^[b] | 219 ^[c] | 192 ^[c] | 194 ^[c] | 180 ^[c] |
| $[4\text{-NO}_2\text{-im}]^-$ | (d) | 232 (283) ^[b] | 220 (253) ^[b] | – | 200 ^[c] | 193 ^[c] | 188 ^[c] | 165 ^[c] |
| $[3,5\text{-diNO}_2\text{-1,2,4-tri}]^-$ | (e) | 368 (402) ^[b] | 284 (321) ^[b] | 277 (296) ^[b] | 239 ^[c] | 219 ^[c] | 205 ^[c] | 235 ^[c] |
| $[2,4\text{-diNO}_2\text{-im}]^-$ | (f) | 339 (379) ^[b] | 281 (317) ^[b] | 258 (281) ^[b] | 254 ^[c] | 221 ^[c] | 216 ^[c] | 222 ^[c] |
| $[4,5\text{-diNO}_2\text{-im}]^-$ | (g) | 279 (322) | 248 (289) | 204 (224) ^[b] | 241 ^[c] | 222 ^[c] | 215 ^[c] | 225 ^[c] |
| $[4,5\text{-diCN-im}]^-$ | (h) | 361 (399) ^[b] | 291 (330) ^[b] | – | 230 ^[c] | 215 ^[c] | 212 ^[c] | 202 ^[c] |
| $[\text{tetr}]^-$ | (i) | 291 (311) ^[b] | 248 (285) ^[b] | – | 208 ^[c] | 180 ^[c] | 184 ^[c] | 198 ^[c] |

[a] Decomposition temperatures shown were determined by TGA, heating at 5°C min^{-1} under dried air atmosphere and are reported as i) onset to 5 wt % mass loss ($T_{5\% \text{ decomp}}$) and ii) onset to total mass loss (T_{decomp}) (in parentheses). [b] T_{onset} data for a second decomposition step at temperature ($^\circ\text{C}$) with percent decomposition (%), respectively: **3a**, 495 (35 %); **3c**, 487 (12 %); **3d**, 490 (18 %); **3e**, 509, (20 %); **3f**, 509 (13 %); **3h**, 528 (14 %); **3i**, 501 (10 %); **4a**, 466 (35 %); **4b**, 497 (17 %); **4c**, 471 (12 %); **4d**, 480 (16 %); **4e**, 535 (8 %); **4f**, 482 (11 %); **4h**, 486 (9 %); **4i**, 500 (10 %); **5a**, 441 (65 %); **5c**, 454 (61 %); **5e**, 486 (59 %); **5f**, 499 (62 %); **5g**, 440 (60 %); **6a**, 499 (36 %); **6b**, 511 (45 %); **9b**, 328 (31 %). [c] Ref. [62].

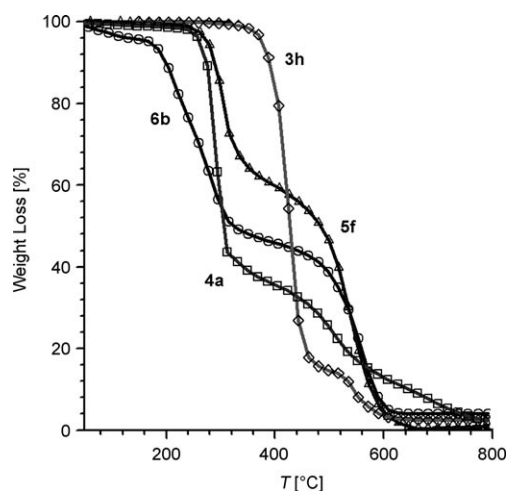


Figure 4. Examples of the observed thermal decomposition with distinguishable two step degradation: $[\text{Ph}_4\text{P}][4,5\text{-diCN-im}]$ **3h** (\diamond), $[\text{Ph}_3\text{EtP}][5\text{-NO}_2\text{-benztri}]$ **4a** (\square), $[\text{N-PhPyr}][2,4\text{-diNO}_2\text{-im}]$ **5f** (Δ), and $[1\text{-Bu-3-Me-im}][5\text{-NO}_2\text{-benzim}]$ **6b** (\circ).

The $[\text{N-PhPyr}]^+$ salts also exhibited two-step decomposition with a broad range first decomposition step between 158–277°C and a narrow second decomposition step between ~440–499°C. The quantity of residue left after the first decomposition step exceeded 60% in all cases (Figure 4, example **5f**). The same two-step decomposition was observed for $[1\text{-Bu-3-Me-im}][5\text{-NO}_2\text{-benztri}]$ **6a** and $[1\text{-Bu-3-Me-im}][5\text{-NO}_2\text{-benzim}]$ **6b** which started decomposition at 177 and 186°C, respectively. The remainder of **6a** (36%) and **6b** (45%) underwent their respective second decomposition steps at 511 and 499°C (Figure 4, example **6b**).

Comparison of the current and previously reported data shown in Table 2, indicated that all tetraalkylammonium and $[1\text{-Bu-3-Me-im}]^+$ salts decompose at much lower temperature ranges, between 141 (**9b**) and 254°C (**6f**), in comparison with their phosphonium, and $[\text{N-PhPyr}]^+$ analogues between 158 (**5a**) and 368°C (**3e**). Unfortunately, the melting points of the new phosphonium salts were higher, although the $[\text{EtPh}_3\text{P}]^+$ salts exhibited relatively lower melting points, similar to those of the tetrabutyl- and tetraethylammonium analogues of the same anions. Thermal stability analyses revealed that again the phosphonium salts exhibited substantially higher temperatures of decomposition (e.g., up to 129°C more stable for **3e** vs **6e**) in comparison with $[1\text{-Bu-3-Me-im}]^+$ and tetraalkylammonium salts.

The type of anions also affected the thermal stabilities observed. In most cases, $[3,5\text{-diNO}_2\text{-tri}]^-$ salts exhibited the highest thermal stabilities with decomposition temperatures as high as 368°C, for **3e**. The high thermal stability, along with the anion's zero oxygen balance (which by definition is the exact amount of oxygen atoms in the molecule to fully oxidize it to CO_2 and H_2O) makes it a very valuable candidate for utilization in energetic ionic liquids and high energy performance materials.

Salts of the structural isomers, $[2,4\text{-diNO}_2\text{-im}]^-$ (**f**) and $[4,5\text{-diNO}_2\text{-im}]^-$ (**g**), were noted to give slightly different

thermal stabilities. The higher thermal stability of salts of $[2,4\text{-diNO}_2\text{-im}]^-$ than $[4,5\text{-diNO}_2\text{-im}]^-$, with a difference in $T_{5\% \text{ decomp}}$ ranging from 2°C for $[\text{Bu}_4\text{N}]^+$ salts, to 89°C for $[\text{Ph}_4\text{P}]^+$ salts, was likely due to the replacement of the C2 hydrogen with a NO_2 group preventing decomposition via cleavage of the C2 hydrogen and further ring decomposition.

In general, for all cation combinations of $[5\text{-NO}_2\text{-benzim}]^-$ (**b**) versus $[5\text{-NO}_2\text{-benztri}]^-$ (**a**) the $[5\text{-NO}_2\text{-benztri}]^-$ (**a**) salts exhibited slight increased thermal stability (and lower melting points for **6a**, **7a**, **8a**, and **9a**). Comparison of $[4\text{-NO}_2\text{-im}]^-$ (**d**) and $[4\text{-NO}_2\text{-tri}]^-$ (**c**) salts yields similar conclusions; the salts of the triazolate core anion tend to exhibit higher decomposition temperatures (up to 42°C) than those of the imidazolate anion.

It was also noted that for the $[\text{Me}_4\text{N}]^+$ salts (**9a–i**), the melting points are either very close to their decomposition temperatures, leaving a very small liquid range before they decompose, or the samples melt at the decomposition point. These experimental results suggest that further tuning of the cation would have to be achieved if these ions were to find specific application.

X-ray crystallography

In total, 19 crystal structures were obtained for the salts studied herein (**3a**, **c–i**; **4a**, **4b**· H_2O , **e–g**, **i**; **5c**, **e**; **7a**· H_2O , **7b**· $0.5\text{H}_2\text{O}$; **9a**) with the most complete series the tetraphenylphosphonium salts of eight of the anions **3a**, **c–i**. Compounds **4e** and **4f** are isostructural. In general and as shown below, the structures can be explained by efficient packing of the ions with modest differences arising from a combination of weak inter-ion interactions (e.g., $\text{C-H}\cdots(\text{N or O})$, π -stacking, etc.) or the presence of a strong hydrogen bond donor water molecule.

The majority of the $[\text{Ph}_4\text{P}]^+$ (**3**) salts crystallize with the cations completely surrounding the anions and all close contacts to the anions being weak $\text{C-H}\cdots(\text{N or O})$ interactions (exclusively these for **3c–f**, **i**) as illustrated in Figure 5 by **3c**. Compound **3a** also has some cation hydrogen atoms (all phenyl) directed toward the more electron-rich portions of the six-membered ring in the anions.

Salts **3g** and **3h** are the only compounds in this series to exhibit anion–anion interactions. The anions in **3g** form linear hydrogen-bonded polymers of the anions via head-to-tail interactions between the acidic ring C-H atom donating to one oxygen each of both nitro substituents in a neighboring anion (Figure 5). Compound **3h** with the cyano rather than nitro substituents, exhibits head-to-head hydrogen bonding between two anions resulting in a dimer (Figure 5). In both cases the remaining interactions with the anions are from the phenyl hydrogen atoms.

The anhydrous $[\text{EtPh}_3\text{P}]^+$ (**4**) salts pack in a similar fashion to the majority of the salts of **3**, that is with anions completely surrounded by cations and a variety of weak C-H interactions (both phenyl C-H or CH_2) with the ring nitrogen atoms and oxygen atoms of the anions (Figure 6). The hy-

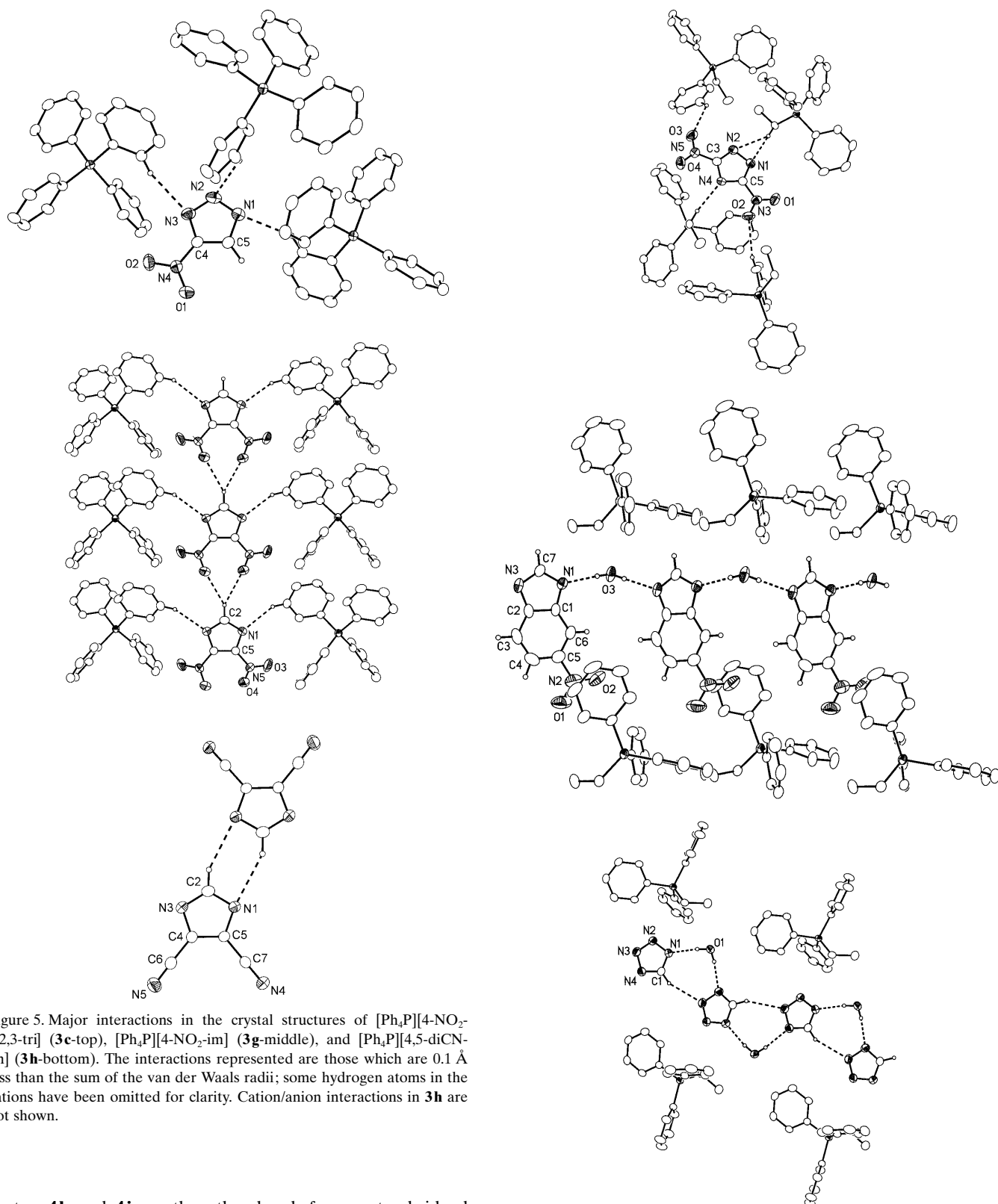


Figure 5. Major interactions in the crystal structures of $[\text{Ph}_4\text{P}][4\text{-NO}_2\text{-1,2,3-tri}]$ (**3c**-top), $[\text{Ph}_4\text{P}][4\text{-NO}_2\text{-im}]$ (**3g**-middle), and $[\text{Ph}_4\text{P}][4,5\text{-diCN-im}]$ (**3h**-bottom). The interactions represented are those which are 0.1 \AA less than the sum of the van der Waals radii; some hydrogen atoms in the cations have been omitted for clarity. Cation/anion interactions in **3h** are not shown.

drates, **4b** and **4i**, on the other hand, form water bridged linear polymers of hydrogen bonded anions (Figure 6). In **4b**, phenyl C–H interactions to the nitro groups complete the close contacts around the anions; however, in **4i** the lone C–H in the anion takes part in anion to anion hydrogen bonding.

Figure 6. Major interactions in the crystal structures of $[\text{EtPh}_3\text{P}][3,5\text{-diNO}_2\text{-1,2,4-tri}]$ (**4e**-top), $[\text{EtPh}_3\text{P}][5\text{-NO}_2\text{-benzim}]\cdot\text{H}_2\text{O}$ (**4b**· H_2O -middle), and $[\text{EtPh}_3\text{P}][\text{tetra}]\cdot 0.5\text{H}_2\text{O}$ (**4i**· $0.5\text{H}_2\text{O}$ -bottom). The interactions represented are those which are 0.1 \AA less than the sum of the van der Waals radii; some hydrogen atoms in the cations have been omitted for clarity.

The geometry of the $[N\text{-PhPyr}]^+$ (**5**) cations should allow some form of classical “ π -stacking” electrostatic interactions with charge-rich regions of the anions and this is indeed observed for **5c** (Figure 7) where the pyridinium portion of the cation resides above and below the plane of the anion at an interplanar distance of 3.48(3) Å to one cation and 3.56(4) Å to another. The pyridinium/phenyl dihedral angle is 107.8(4)° indicating a serve twist of these rings.

Interestingly, in **5e** the anions exhibit offset stacking with each other (Figure 7) rather than with the cations and the interplanar spacings are longer at about 3.812(1) Å. The close contacts of the cation with the anions are via weak C–H interactions and in this case, the dihedral angle between the phenyl and pyridinium planes is only 41.6(5)°.

The two $[\text{Bu}_4\text{N}]^+$ (**7**) salts, both hydrates, exhibit interesting packing behavior as illustrated in Figure 8. Compound **7a** (a monohydrate) crystallizes with planes of water bridged, hydrogen bonded anion dimers separating planes of flattened $[\text{Bu}_4\text{N}]^+$ cations, while in **7b** (a hemihydrate), the water molecules bridge hydrogen bonded anion dimers forming corrugated sheets of anions which separate the cation layers.

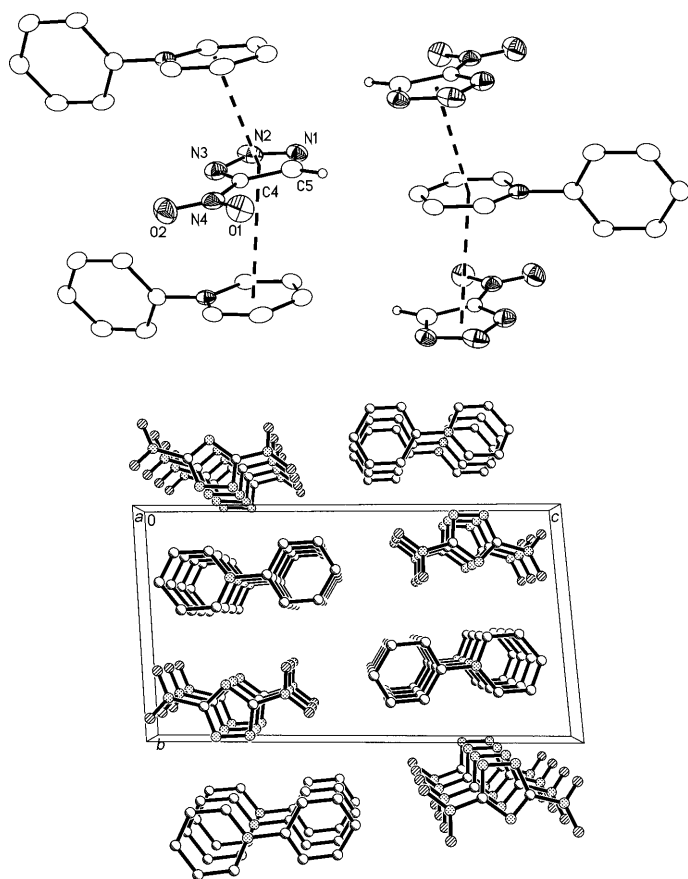


Figure 7. The nature of the different stacking interactions observed in the crystal structures of $[N\text{-PhPyr}][4\text{-NO}_2\text{-1,2,3-tri}]$ (**5c**-top) and $[N\text{-PhPyr}][4\text{-NO}_2\text{-1,2,3-tri}]$ (**5e**-bottom). The interactions represented are those which are 0.1 Å less than the sum of the van der Waals radii; some hydrogen atoms in the cations have been omitted for clarity.

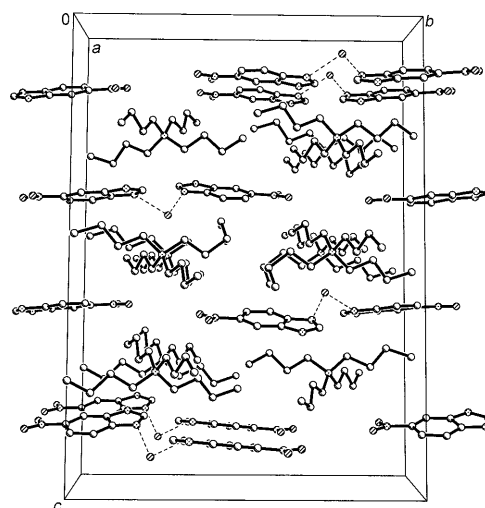
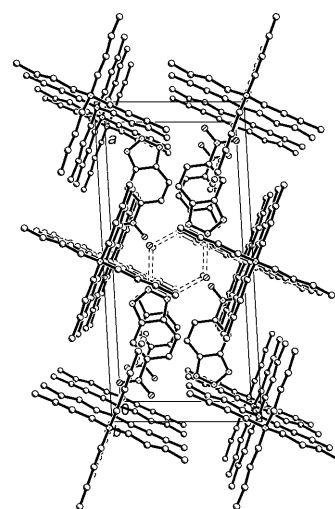
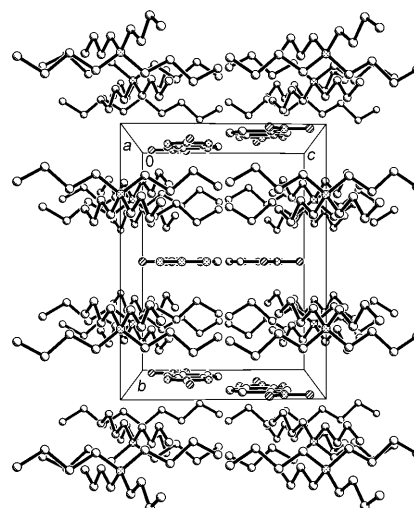


Figure 8. Crystal packing diagrams for $[\text{Bu}_4\text{N}][5\text{-NO}_2\text{-benztri}]$ (**7a** down *a* axis (top) and down *b* axis (middle)) and $[\text{Bu}_4\text{N}][5\text{-NO}_2\text{-benzim}]$ (**7b**-bottom). Only the water hydrogen bonds are shown; hydrogen atoms have been omitted for clarity.

The only $[\text{Me}_4\text{N}]^+$ structure obtained, **9a**, has a relatively salt like structure, although the anions do stack with a nitro group from a neighboring anion above and below the electron-rich phenyl ring at a distance of 3.72(1) Å (Figure 9). All remaining close contacts to these anions are from the cation hydrogen atoms.

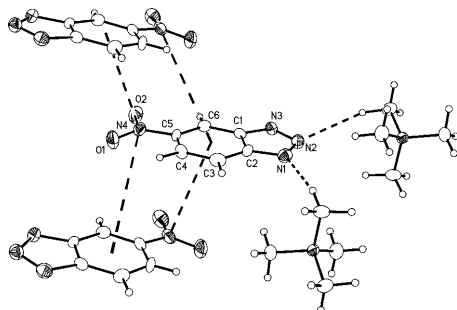


Figure 9. The anion environment in $[\text{Me}_4\text{N}][5\text{-NO}_2\text{-benztri}]$ (**9a**).

While in general the variation in the structures is interesting, there is little yet to allow us to point to specific interactions which might be responsible for observed physical properties or which could be used to predict performance when combined with other ions. Nonetheless, we will continue to analyze such structures in the hope that a larger database of available crystal structures might ultimately provide theoretical chemists with sufficient ammunition to be able to predict properties from knowledge of the component ions alone.

Conclusions

We have studied a series of salts to gain insight in how energetic functionalities might be introduced into potential EILs while retaining key physical properties desired for application. Electron-withdrawing groups, such as nitro or nitrile, may act as destabilizing substituents on the aromatic core of many heterocyclic cations, as well as stabilizing substituents on many heterocyclic anions, and a wide range of azolate anion-based salts can thus be used to prepare EILs. Here we have presented 31 such examples. The azolates have been found to not only introduce properties required for EILs, but also allow for the formation of low melting salts, and indeed in some cases ILs. They are surprisingly stable in the systems explored, and allow a degree of structural modification in a similar fashion to azolium cations.

Ionic liquids were obtained with all combinations of $[1\text{-Bu-3-Me-im}]^+$ and the heterocyclic azolate anions studied, and with several combinations of $[\text{Bu}_4\text{N}]^+$ or $[\text{Et}_4\text{N}]^+$. The $[1\text{-Bu-3-Me-im}]^+$ azolates were liquid at room temperature, forming glasses on cooling with transition temperatures in the range -53 to -82°C (except for the $[3,5\text{-diNO}_2\text{-tri}]^-$ salt, m.p. 33°C). Additionally, one of the most interesting findings was that the melting points and thermal stabilities of the $[1\text{-Bu-3-Me-im}]^+$ salts allow for handling, operation, and usage over a wide liquidus range (Figure 10).

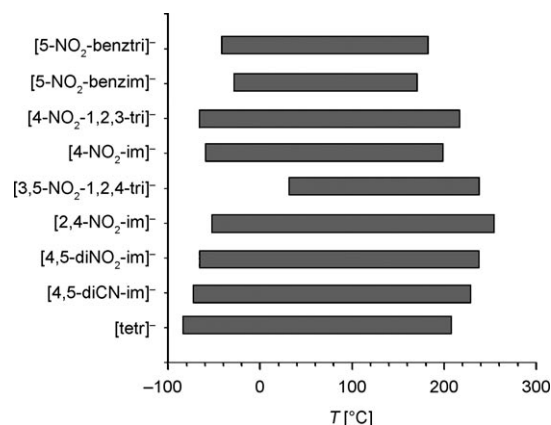


Figure 10. Liquidus ranges of the $[1\text{-Bu-3-Me-im}]^+$ salts.

Taking into the account the specific properties analyzed (liquid range, thermal stability, oxygen balance) the most promising anion for the application in energetic ionic liquids seems to be $[3,5\text{-diNO}_2\text{-tri}]^-$. Other trends discovered (Table 3) include favorable structure–property relationships when moving from 4- and 4,5-disubstituted anions to 3,5- and 2,4-disubstituted azolate anions. For example, it was found that the $[2,4\text{-diNO}_2\text{-im}]^-$ anion contributes to low melting point, very good thermal stabilities, high oxygen balance, high nitrogen content, and high solid-state density for most of the analyzed salts. Overall, the development of ILs based on azolium azolate cores seems to be an attractive avenue for the future of not only energetic ionic liquids, but ILs in general.

Experimental Section

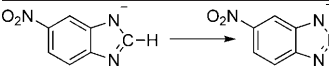

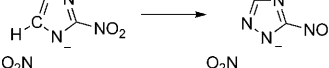
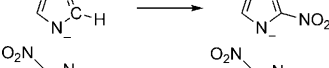


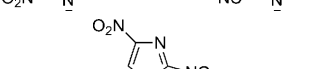
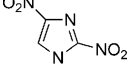
General methods: The melting points were determined using both a hot stage apparatus (presented in the experimental section), as well as a differential scanning calorimeter (DSC; shown only in the Table 1). The discrepancy between some of the melting points in Table 1 and in the experimental section arises from the analysis of the salts prior to recrystallization (typically a hydrate) and often corresponds to a first irreversible thermal transition obtained by DSC reported in Table 1.

NMR spectra were obtained in CDCl_3 (unless otherwise stated) with TMS as the internal standard for ^1H (300 MHz) or the solvent as the internal standard for ^{13}C (75 MHz). All of the chemicals were employed as supplied. It should be noted that in the syntheses of these new materials, the presence of compounds that precipitated as hydrates were first recognized in elemental analyses, and then further found in the crystal structures, as monohydrates or anhydrous salts.

Materials: Potassium 3,5-dinitro-1,2,4-triazolate was prepared according to the published one-pot procedure by the reaction of cyanoguanidine with hydrazine followed by diazotization of intermediate 3,5-diamino-1H-triazole and substitution at the diazonium group in 46% yield.^[70] 4-Nitro-2H-1,2,3-triazole was prepared according to a published procedure from 2-phenyl-2H-1,2,3-triazole by the trinitration followed by treatment of intermediate 2-(2,4-dinitrophenyl)-4-nitro-2H-1,2,3-triazole with sodium methoxide in methanol under reflux.^[71] 2,4-Dinitroimidazole m.p. $260\text{--}263^\circ\text{C}$ (lit. $264\text{--}267^\circ\text{C}$)^[72] was prepared by N-nitration of 4-nitroimidazole followed by isomerization of the intermediate 1,4-dinitroimidazole in chlorobenzene at 115°C .^[73,74]

Procedure for the preparation of 4,5-dinitroimidazole (1g): To 4-nitroimidazole (2.0 g, 18 mmol) dissolved in a minimum quantity of concentrated

Table 3. Summary of structure–property relationships.

| Structure–property relationship | m.p. | T_{decomp} | Oxygen balance (OB) ^[a] | Nitrogen content ^{[b],[69]} | Solid density |
|-----------------------------------------------------------------------------------|------------------------|------------------------|------------------------------------|--------------------------------------|-----------------------------------------------------|
| | ↓ | ↑ | ↑ | ↑ | ↑ |
| Desired change in property | | | | | |
|  | data inconclusive | ↑ | ↑ | ↑ | – |
|  | ↓ | ↑ | ↑ | ↑ | ↓ |
|  | ↑ | ± 29 °C ^[c] | ↑ | ↑ | ↑ |
|  | ± 38 °C ^[d] | ↑ | ↑ | ↓ | ↑ |
|  | ↓ | ↑ | ↑ | ↓ | = |
|  | ± 50 °C ^[d] | ↑ | = | = | ↑ |
|  | ± 36 °C ^[d] | ± 43 °C ^[c] | ↓ | ↑ | ↓ |
|  | moderate 33–214 °C | high 205–368 °C | highest +0 | high 44.3 % | high ^[e] 1.36–1.55 g cm ^{–3} |

[a] The oxygen balance (OB) is calculated from the empirical formula of a compound in percentage of oxygen required for complete conversion of carbon to carbon dioxide, hydrogen to water, and metal to metal oxide.

[b] Nitrogen content is defined as the amount of nitrogen in the molecule expressed in mass %. [c] Maximum variation in temperature of melting point between salts of considered set of anions. [d] Maximum variation in temperature of decomposition between salts of considered set of anions. [e] The [3,5-diNO₂-tri][–] anion contributes to one of the higher densities among the analyzed family of salts.

sulfuric acid was added a mixture of concentrated sulfuric acid (10 mL) and fuming nitric acid (90 %, 8 mL, 0.17 mol). The mixture was heated under reflux for 5 h. After cooling, the mixture was poured into ice, and the pH was adjusted to 2 by the addition of sodium bicarbonate. The product was extracted with ethyl acetate. The extract was concentrated to give 4,5-dinitroimidazole as yellow crystals from water (1.55 g, 55 %). M.p. 166–169 °C (lit. 188–189 °C);^[74] ¹H NMR ([D₆]DMSO): δ = 12.37 (brs, 1H), 8.06 ppm (s, 1H); ¹³C NMR ([D₆]DMSO): δ = 135.5, 134.9.

General procedure for the preparation of potassium azolates 2a–c, e–g: Potassium carbonate (0.85 g, 6 mmol) was added to a solution of appropriate azole (4 mmol) in acetone (40 mL) (Scheme 1). The mixture was stirred at 20 °C for 6 h, filtered and the precipitate was washed with acetone. The solvent was evaporated and the residue was dried under vacuum to give potassium azolates 2a–c, e–g.

General procedure for the preparation of azolates 3–9a–b and 3–5c, e–g: A solution of appropriate tetraphenylphosphonium, ethyltriphenylphosphonium, *N*-phenylpyridinium, 1-butyl-3-methylimidazolium, or tetraalkylammonium halide (2 mmol) in dichloromethane (30 mL) was added to a solution of potassium azolate 2a–c, e–g (2 mmol) in acetone (30 mL) at 20–25 °C. The reaction mixture was stirred for 3 h, but 24 h for the preparation of tetramethylammonium salts. The resultant potassium halide precipitate was removed by filtration and the solvent was evaporated under vacuum. The residue was dried under vacuum. The product was extracted with acetone, the extract was filtered, and the solvent was removed to give 3–9a–b and 3–5c, e–g.

General procedure for the preparation of azolates 3–4d, h–i: Anhydrous potassium carbonate (0.7 g, 5 mmol) was added to a solution of appropriate azole (2 mmol) in acetone (30 mL) and the mixture was stirred for 30 min at 20–25 °C. Then a solution of tetraphenylphosphonium, ethyltri-

phenylphosphonium, or *N*-phenylpyridinium halide (2 mmol) in dichloromethane (30 mL) was added and the reaction mixture was stirred for 3 h. The mixture was filtered and concentrated under vacuum. The product was extracted with acetone, the extract was filtered, and the solvent was removed to give 3–4d, h–i.

Tetraphenylphosphonium 5-nitrobenzotriazole (3a) monohydrate: Microcrystals from acetone (95 %), m.p. 141–143 °C (DSC 2nd cycle m.p. 145 °C); ¹H NMR (CDCl₃): δ = 7.46–7.53 (m, 8H), 7.65–7.74 (m, 9H), 7.77–7.86 (m, 5H), 8.67 ppm (d, *J* = 1.8 Hz, 1H); ¹³C NMR (CDCl₃): δ = 114.5 (d, *J* = 2.3 Hz, 1C), 115.1, 116.0, 117.1 (d, *J* = 89.9 Hz, 4C), 130.5 (d, *J* = 12.6 Hz, 8C), 134.1 (d, *J* = 10.3 Hz, 8C), 135.6 (d, *J* = 3.4 Hz, 4C), 141.2, 144.4, 148.6 ppm; elemental analysis calcd (%) for C₃₀H₂₅N₄O₃P: C 69.22, H 4.84, N 10.76; found: C 70.16, H 4.47, N 11.15.

Tetraphenylphosphonium 5-nitrobenzimidazole (3b) monohydrate: Colorless oil (91 %); DSC m.p. 55 °C; ¹H NMR (CDCl₃): δ = 7.53–7.60 (m, 9H), 7.71–7.77 (m, 8H), 7.86–7.91 (m, 5H), 8.27 (s, 1H), 8.50 (d, *J* = 1.6 Hz, 1H); ¹³C NMR (CDCl₃): δ = 113.4, 114.8, 115.6, 117.1 (d, *J* = 89.9 Hz, 4C), 130.5 (d, *J* = 13.2 Hz, 8C), 134.0 (d, *J* = 10.3 Hz, 8C), 135.6 (d, *J* = 2.9 Hz, 4C), 140.9, 142.0, 146.9, 152.1 ppm; elemental analysis calcd (%) for C₃₁H₂₆N₃O₃P: C 71.67, H 5.04, N 8.09; found: C 70.55, H 4.78, N 8.47.

Tetraphenylphosphonium 4-nitro-1,2,3-triazolate (3c) monohydrate: Light yellow microcrystals from acetone (95 %), m.p. 157–159 °C (DSC 2nd cycle m.p. 155 °C); ¹H NMR (CDCl₃): δ = 7.56–7.63 (m, 8H), 7.72–7.78 (m, 8H), 7.86–7.91 (m, 4H), 8.05 ppm (s, 1H); ¹³C NMR (CDCl₃): δ = 117.1 (d, *J* = 89.3 Hz, 4C), 130.0, 130.5 (d, *J* = 13.2 Hz, 8C), 134.1 (d, *J* = 11.3 Hz, 8C), 135.6 (d, *J* = 2.8 Hz, 4C), 154.4; elemental analysis calcd (%) for C₂₆H₂₃N₄O₃P: C 66.38, H 4.93, N 11.91; found: C 66.08, H 4.36, N 13.51.

Tetraphenylphosphonium 4-nitroimidazole (3d): Microcrystals from acetone (94 %), m.p. 162–165 °C (DSC 2nd cycle m.p. 171 °C); ¹H NMR (CDCl₃): δ = 7.29 (s, 1H), 7.54–7.62 (m, 8H), 7.70–7.76 (m, 8H), 7.84–7.90 ppm (m, 5H); ¹³C NMR (CDCl₃): δ = 117.2 (d, *J* = 89.3 Hz, 4C), 130.5 (d, *J* = 12.6 Hz, 8C), 132.1, 134.1 (d, *J* = 10.3 Hz, 8C), 135.6 (d, *J* = 3.4 Hz, 4C), 146.7, 146.7 ppm; elemental analysis calcd (%) for C₂₇H₂₂N₃O₂P: C 71.83, H 4.91, N 9.31; found: C 71.01, H 4.79, N 9.24.

Tetraphenylphosphonium 3,5-dinitro-1,2,4-triazolate (3e): Microcrystals from acetone (99 %), m.p. 175–178 °C (DSC 2nd cycle m.p. 171 °C); ¹H NMR (CDCl₃): δ = 7.58–7.65 (m, 8H), 7.73–7.79 (m, 8H), 7.87–7.92 ppm (m, 4H); ¹³C NMR (CDCl₃): δ = 117.2 (d, *J* = 89.9 Hz, 4C), 130.5 (d, *J* = 13.1 Hz, 8C), 134.2 (d, *J* = 10.3 Hz, 8C), 135.6 (d, *J* = 2.9 Hz, 4C), 163.2 ppm; elemental analysis calcd (%) for C₂₆H₂₀N₅O₄P: C 62.78, H 4.05, N 14.08; found: C 62.65, H 3.88, N 14.26.

Tetraphenylphosphonium 2,4-dinitroimidazole (3f): Microcrystals from acetone (90 %), m.p. 195–197 °C (DSC 2nd cycle m.p. 191 °C); ¹H NMR (CDCl₃): δ = 7.57–7.64 (m, 8H), 7.67 (s, 1H), 7.72–7.78 (m, 8H), 7.86–7.91 ppm (m, 4H); ¹³C NMR (CDCl₃): δ = 117.2 (d, *J* = 89.9 Hz, 4C), 130.3, 130.5 (d, *J* = 12.6 Hz, 8C), 134.1 (d, *J* = 10.9 Hz, 8C), 135.6 (d, *J* = 2.9 Hz, 4C), 147.1, 154.2 ppm; elemental analysis calcd (%) for C₂₇H₂₁N₄O₄P: C 65.32, H 4.26, N 11.29; found: C 64.48, H 4.18, N 11.26.

Tetraphenylphosphonium 4,5-dinitroimidazolate (3g): Microcrystals from acetone (92 %), m.p. 159–162 °C (DSC 2nd cycle m.p. 145 °C); ¹H NMR (CDCl₃): δ = 7.00 (s, 1H), 7.58–7.65 (m, 8H), 7.72–7.79 (m, 8H), 7.88–7.93 ppm (m, 4H); ¹³C NMR (CDCl₃): δ = 116.9 (d, *J* = 89.9 Hz, 4C), 130.3 (d, *J* = 12.6 Hz, 8C), 133.9 (d, *J* = 10.3 Hz, 8C), 135.4 (d, *J* = 2.8 Hz, 4C), 139.5, 139.6, 140.3 ppm; elemental analysis calcd (%) for C₂₇H₂₁N₄O₄P: C 65.32, H 4.26, N 11.29; found: C 64.37, H 4.05, N 11.37.

Tetraphenylphosphonium 4,5-dicyanoimidazolate (3h): Microcrystals from acetone (88 %), m.p. 157–159 °C (DSC 2nd cycle m.p. 149 °C); ¹H NMR (CDCl₃): δ = 7.37 (s, 1H), 7.56–7.64 (m, 8H), 7.71–7.78 (m, 8H), 7.87–7.92 ppm (m, 4H); ¹³C NMR (CDCl₃): δ = 116.9, 117.2 (d, *J* = 89.4 Hz, 4C), 130.5 (d, *J* = 13.2 Hz, 8C), 134.1 (d, *J* = 10.3 Hz, 8C), 135.6 (d, *J* = 3.4 Hz, 4C), 148.9, 148.9 ppm; elemental analysis calcd (%) for C₂₉H₂₁N₄P: C 76.30, H 4.64, N 12.27; found: C 75.42, H 4.46, N 12.74.

Tetraphenylphosphonium tetrazolate (3i) monohydrate: Microcrystals from acetone (85 %), m.p. 308–311 °C (DSC m.p. at *T*_{decomp} 290 °C); ¹H NMR (CDCl₃): δ = 7.55–7.62 (m, 8H), 7.71–7.78 (m, 8H), 7.88–7.91 (m, 4H), 8.31 ppm (s, 1H); ¹³C NMR (CDCl₃): δ = 117.1 (d, *J* = 89.4 Hz, 4C), 130.5 (d, *J* = 13.2 Hz, 8C), 134.0 (d, *J* = 10.3 Hz, 8C), 135.5 (d, *J* = 3.4 Hz, 4C), 149.6 (d, *J* = 2.9 Hz, 1C); elemental analysis calcd (%) for C₂₅H₂₁N₄O₃P: C 70.41, H 5.44, N 13.14; found: C 71.64, H 5.04, N 13.52.

Ethyltriphenylphosphonium 5-nitrobenzotriazolate (4a) monohydrate: Light brown microcrystals from acetone (99 %); m.p. 120–122 °C (DSC 2nd cycle m.p. 131 °C); ¹H NMR (CDCl₃): δ = 1.29 (dt, *J* = 19.8, 7.5 Hz, 3H), 3.18–3.30 (m, 2H), 7.51–7.65 (m, 12H), 7.72–7.85 (m, 4H), 7.83 (dd, *J* = 9.0, 2.2 Hz, 1H), 8.65 ppm (d, *J* = 2.2 Hz, 1H); ¹³C NMR (CDCl₃): δ = 6.6, 16.3 (d, *J* = 52.7 Hz, 1C), 114.3 (d, *J* = 3.4 Hz, 1C), 115.2, 115.9, 117.2 (d, *J* = 86.4 Hz, 3C), 130.3 (d, *J* = 12.0 Hz, 6C), 133.0 (d, *J* = 9.8 Hz, 6C), 135.1 (d, *J* = 2.8 Hz, 3C), 141.3, 144.3, 148.5 ppm; elemental analysis calcd (%) for C₂₆H₂₅N₄O₃P: C 66.09, H 5.33, N 11.86; found: C 65.56, H 4.89, N 11.35.

Ethyltriphenylphosphonium 5-nitrobenzimidazolate (4b) monohydrate: Red oil (98 %); DSC 1st cycle m.p. 88 °C; ¹H NMR (CDCl₃): δ = 1.28 (dt, *J* = 19.8, 7.4 Hz, 3H), 3.15 (dq, *J* = 12.6, 7.4 Hz, 2H), 7.50–7.58 (m, 7H), 7.61–7.68 (m, 6H), 7.76–7.81 (m, 3H), 7.89 (dd, *J* = 8.8, 2.2 Hz, 1H), 8.26 (s, 1H), 8.48 ppm (d, *J* = 2.2 Hz, 1H); ¹³C NMR (CDCl₃): δ = 6.4, 16.3 (d, *J* = 52.1 Hz, 1C), 113.5, 114.1, 115.2, 117.2 (d, *J* = 85.9 Hz, 3C), 130.3 (d, *J* = 12.6 Hz, 6C), 132.9 (d, *J* = 9.7 Hz, 6C), 135.1 (d, *J* = 2.9 Hz, 3C), 139.2, 144.8, 151.8, 158.1 ppm; elemental analysis calcd (%) for C₂₇H₂₆N₄O₃P: C 68.78, H 5.13, N 8.91; found: C 67.43, H 5.61, N 7.94.

Ethyltriphenylphosphonium 4-nitro-1,2,3-triazolate (4c): Light yellow microcrystals from acetone (99 %); m.p. 90–92 °C (DSC 2nd cycle m.p. 97 °C); ¹H NMR (CDCl₃): δ = 1.38 (dt, *J* = 19.8, 7.4 Hz, 3H), 3.44 (dq, *J* = 12.8, 7.5 Hz, 2H), 7.65–7.72 (m, 12H), 7.70–7.84 (m, 3H), 8.07 ppm (s, 1H); ¹³C NMR (CDCl₃): δ = 6.6 (d, *J* = 5.2 Hz, 1C), 16.4 (d, *J* = 52.7 Hz, 1C), 117.4 (d, *J* = 86.5 Hz, 3C), 130.1, 130.4 (d, *J* = 12.6 Hz, 6C), 133.2 (d, *J* = 9.7 Hz, 6C), 135.1 (d, *J* = 2.9 Hz, 3C), 154.5 ppm; elemental analysis calcd (%) for C₂₂H₂₁N₄O₂P: C 65.34, H 5.23, N 13.85; found: C 64.36, H 5.13, N 13.71.

Ethyltriphenylphosphonium 4-nitroimidazolate (4d) monohydrate: Light yellow microcrystals from acetone (98 %); m.p. 89–91 °C (DSC 2nd cycle m.p. 100 °C); ¹H NMR (CDCl₃): δ = 1.35 (dt, *J* = 19.8, 7.4 Hz, 3H), 3.44 (dq, *J* = 12.7, 7.5 Hz, 2H), 7.28 (s, 1H), 7.60–7.72 (m, 12H), 7.78–7.84 (m, 3H), 7.89 ppm (s, 1H); ¹³C NMR (CDCl₃): δ = 6.5 (d, *J* = 5.2 Hz, 1C), 16.3 (d, *J* = 52.7 Hz, 1C), 117.3 (d, *J* = 86.2 Hz, 3C), 130.4 (d, *J* = 12.6 Hz, 6C), 132.3, 133.1 (d, *J* = 10.3 Hz, 6C), 135.1 (d, *J* = 2.9 Hz, 3C), 146.7 (d, *J* = 4.0 Hz, 1C), 148.3 ppm; elemental analysis calcd (%) for C₂₃H₂₄N₄O₃P: C 65.55, H 5.74, N 9.97; found: C 66.57, H 5.40, N 9.85.

Ethyltriphenylphosphonium 3,5-dinitro-1,2,4-triazolate (4e): Microcrystals from acetone (96 %), m.p. 124–125 °C (DSC 2nd cycle m.p. 127 °C); ¹H NMR (CDCl₃): δ = 1.44 (dt, *J* = 19.8, 7.6 Hz, 3H), 3.38 (dq, *J* = 12.6, 7.4 Hz, 2H), 7.64–7.75 (m, 12H), 7.79–7.86 ppm (m, 3H); ¹³C NMR (CDCl₃): δ = 6.6 (d, *J* = 5.7 Hz, 1C), 16.6 (d, *J* = 53.3 Hz, 1C), 117.2 (d, *J* = 86.5 Hz, 3C), 130.5 (d, *J* = 12.6 Hz, 6C), 133.2 (d, *J* = 9.7 Hz, 6C), 135.3 (d, *J* = 3.5 Hz, 3C), 163.2 ppm; elemental analysis calcd (%) for C₂₂H₂₀N₅O₄P: C 58.80, H 4.49, N 15.58; found: C 58.63, H 4.35, N 15.19.

Ethyltriphenylphosphonium 2,4-dinitroimidazolate (4f) monohydrate: Light yellow microcrystals from acetone (96 %); m.p. 68–70 °C (DSC 1st cycle m.p. 70 °C); ¹H NMR (CDCl₃): δ = 1.41 (dt, *J* = 19.6, 7.4 Hz, 3H), 3.39 (dq, *J* = 12.6, 7.4 Hz, 2H), 7.63–7.74 (m, 13H), 7.78–7.86 ppm (m, 3H); ¹³C NMR (CDCl₃): δ = 6.5, 16.4 (d, *J* = 53.3 Hz, 1C), 117.1 (d, *J* = 85.9 Hz, 3C), 130.3, 130.4 (d, *J* = 12.6 Hz, 6C), 133.0 (d, *J* = 9.6 Hz, 6C), 135.1 (d, *J* = 2.9 Hz, 3C), 147.0, 154.1 ppm; elemental analysis calcd (%) for C₂₃H₂₃N₄O₃P: C 59.23, H 4.97, N 12.01; found: C 60.29, H 4.64, N 11.40.

Ethyltriphenylphosphonium 4,5-dinitroimidazolate (4g): Yellow microcrystals from acetone (95 %); m.p. 91–93 °C (DSC 1st cycle m.p. 97 °C); ¹H NMR (CDCl₃): δ = 1.39 (dt, *J* = 19.8, 7.4 Hz, 3H), 3.25 (dq, *J* = 12.7, 7.5 Hz, 2H), 7.00 (s, 1H), 7.59–7.73 (m, 12H), 7.79–7.85 ppm (m, 3H); ¹³C NMR (CDCl₃): δ = 6.6, 16.6 (d, *J* = 52.7 Hz, 1C), 117.2 (d, *J* = 86.4 Hz, 3C), 130.5 (d, *J* = 12.6 Hz, 6C), 133.2 (d, *J* = 9.7 Hz, 6C), 135.3 (d, *J* = 3.5 Hz, 3C), 139.8 (d, *J* = 5.7 Hz, 1C), 140.6 ppm; elemental analysis calcd (%) for C₂₃H₂₁N₄O₄P: C 61.61, H 4.72, N 12.49; found: C 61.33, H 4.74, N 12.36.

Ethyltriphenylphosphonium 4,5-dicyanoimidazolate (4h): Light yellow oil (96 %); DSC 2nd cycle m.p. –29 °C; ¹H NMR (CDCl₃): δ = 1.40 (dt, *J* = 19.5, 7.3 Hz, 3H), 3.21 (dq, *J* = 12.7, 7.4 Hz, 2H), 7.39 (s, 1H), 7.59–7.66 (m, 6H), 7.68–7.74 (m, 6H), 7.81–7.86 ppm (m, 3H); ¹³C NMR (CDCl₃): δ = 6.6, 16.6 (d, *J* = 53.2 Hz, 1C), 116.9, 117.1 (d, *J* = 85.9 Hz, 3C), 118.4, 130.5 (d, *J* = 12.6 Hz, 6C), 133.1 (d, *J* = 9.7 Hz, 6C), 135.4 (d, *J* = 3.4 Hz, 3C), 148.9 ppm (d, *J* = 8.0 Hz, 1C); elemental analysis calcd (%) for C₂₅H₂₁N₄P: C 73.52, H 5.18, N 13.72; found: C 72.87, H 5.33, N 13.44.

Ethyltriphenylphosphonium tetrazolate (4i) monohydrate: Light yellow microcrystals from acetone (89 %); m.p. 83–85 °C (DSC 1st cycle m.p. 51 °C); ¹H NMR (CDCl₃): δ = 1.32 (dt, *J* = 20.0, 7.6 Hz, 3H), 3.38 (dq, *J* = 12.7, 7.8 Hz, 2H), 7.62–7.72 (m, 12H), 7.76–7.82 (m, 3H), 8.30 ppm (s, 1H); ¹³C NMR (CDCl₃): δ = 6.4 (d, *J* = 5.2 Hz, 1C), 16.0 (d, *J* = 52.7 Hz, 1C), 117.5 (d, *J* = 85.9 Hz, 3C), 130.3 (d, *J* = 12.6 Hz, 6C), 133.1 (d, *J* = 10.3 Hz, 6C), 134.9 (d, *J* = 2.9 Hz, 3C), 149.6 ppm (d, *J* = 4.0 Hz, 1C); elemental analysis calcd (%) for C₂₁H₂₃N₄O₃P: C 66.65, H 6.13, N 14.81; found: C 66.87, H 5.94, N 14.57.

N-Phenylpyridinium 5-nitrobenzotriazolate (5a) monohydrate: Black microcrystals from acetone (96 %); m.p. 79–81 °C (DSC 1st cycle m.p. 75 °C); ¹H NMR ([D₆]DMSO): δ = 7.73–7.76 (m, 4H), 7.83 (dd, *J* = 9.0, 2.1 Hz, 1H), 7.88–7.92 (m, 2H), 8.29–8.34 (m, 2H), 8.62 (d, *J* = 2.0 Hz, 1H), 8.79 (t, *J* = 7.8 Hz, 1H), 9.36 ppm (d, *J* = 5.6 Hz, 2H); ¹³C NMR ([D₆]DMSO): δ = 113.5 (d, *J* = 3.4 Hz, 1C), 115.0, 115.7, 124.7, 128.1, 130.2, 131.2, 140.7, 142.8, 143.8, 144.9, 146.6, 147.8 ppm; elemental analysis calcd (%) for C₁₇H₁₅N₅O₃: C 60.53, H 4.48, N 20.76; found: C 59.92, H 4.21, N 21.11.

N-Phenylpyridinium 4-nitro-1,2,3-triazolate (5c): Microcrystals from acetone (94 %); m.p. 129–131 °C (DSC 2nd cycle m.p. 135 °C); ¹H NMR ([D₆]DMSO): δ = 7.73–7.76 (m, 3H), 7.89–7.92 (m, 2H), 8.02 (s, 1H), 8.30–8.34 (m, 2H), 8.80 (t, *J* = 7.8 Hz, 1H), 9.36 ppm (d, *J* = 5.5 Hz, 2H); ¹³C NMR ([D₆]DMSO): δ = 124.7, 128.1, 129.5, 130.2, 131.2, 142.8, 144.9, 146.6, 154.1 ppm; elemental analysis calcd (%) for C₁₃H₁₁N₅O₂: C 57.99, H 4.12, N 26.01; found: C 57.75, H 3.95, N 26.28.

N-Phenylpyridinium 3,5-dinitro-1,2,4-triazolate (5e): Microcrystals from acetone (88 %); m.p. 158–160 °C (DSC 2nd cycle m.p. 167 °C); ¹H NMR ([D₆]DMSO): δ = 7.73–7.77 (m, 3H), 7.88–7.92 (m, 2H), 8.30–8.35 (m, 2H), 8.80 (t, *J* = 7.8 Hz, 1H), 9.36 ppm (d, *J* = 5.5 Hz, 2H); ¹³C NMR ([D₆]DMSO): δ = 124.7, 128.1, 130.2, 131.2, 142.8, 145.0, 146.6, 162.9 ppm; elemental analysis calcd (%) for C₁₃H₁₀N₆O₄: C 49.69, H 3.21, N 26.74; found: C 49.53, H 2.99, N 26.27.

N-Phenylpyridinium 2,4-dinitroimidazolate (5f): Light yellow microcrystals from acetone (93 %), m.p. 140–142 °C (DSC 2nd cycle m.p. 143 °C); ¹H NMR ([D₆]DMSO): δ = 7.71 (s, 1H), 7.74–7.77 (m, 3H), 7.89–7.92 (m, 2H), 8.30–8.35 (m, 2H), 8.80 (t, *J* = 7.8 Hz, 1H), 9.37 ppm (d, *J* = 5.7 Hz, 2H); ¹³C NMR ([D₆]DMSO): δ = 100.1, 124.8, 128.1, 130.2, 130.3, 131.2, 142.8, 145.0, 146.6, 146.8 ppm; elemental analysis calcd (%) for C₁₄H₁₁N₅O₄: C 53.68, H 3.54, N 22.36; found: C 53.99, H 3.40, N 22.29.

N-Phenylpyridinium 4,5-dinitroimidazole (5g): Light brown microcrystals from acetone (91%), m.p. 129–132°C (DSC 2nd cycle m.p. 140°C); ^1H NMR ($[\text{D}_6]\text{DMSO}$): δ = 6.94 (s, 1H), 7.74–7.77 (m, 3H), 7.88–7.91 (m, 2H), 8.29–8.34 (m, 2H), 8.79 (t, J = 7.8 Hz, 1H), 9.36 ppm (d, J = 5.8 Hz, 2H); ^{13}C NMR ($[\text{D}_6]\text{DMSO}$): δ = 124.7, 128.1, 130.2, 131.2, 139.3, 139.4, 142.8, 145.0, 146.5 ppm; elemental analysis calcd (%) for $\text{C}_{14}\text{H}_{11}\text{N}_5\text{O}_4$: C 53.68, H 3.54, N 22.36; found: C 53.45, H 3.34, N 22.29.

1-Butyl-3-methylimidazolium 5-nitrobenzotriazole (6a): Colorless oil (94%); DSC 2nd cycle T_g = -41°C ; ^1H NMR (CDCl_3): δ = 0.83 (t, J = 7.3 Hz, 3H), 1.15–1.28 (m, 2H), 1.66–1.76 (m, 2H), 3.92 (s, 3H), 4.09 (t, J = 7.4 Hz, 2H), 7.24 (t, J = 1.8 Hz, 1H), 7.28 (t, J = 1.6 Hz, 1H), 7.82 (d, J = 8.9 Hz, 1H), 7.94 (dd, J = 8.9, 2.1 Hz, 1H), 8.78 (d, J = 2.1 Hz, 1H), 9.81 ppm (s, 1H); ^{13}C NMR (CDCl_3): δ = 13.1, 19.2, 31.7, 36.2, 49.7, 114.2, 116.0, 116.1, 121.8, 123.2, 137.2, 142.0, 144.2, 148.3 ppm; elemental analysis calcd (%) for $\text{C}_{14}\text{H}_{18}\text{N}_6\text{O}_2$: C 55.62, H 6.00, N 27.80; found: C 54.65, H 6.16, N 27.00.

1-Butyl-3-methylimidazolium 5-nitrobenzimidazole (6b) monohydrate: Colorless oil (98%); DSC 2nd cycle T_g = -34°C ; ^1H NMR (CDCl_3): δ = 0.87 (t, J = 7.3 Hz, 3H), 1.16–1.29 (m, 2H), 1.64–1.74 (m, 2H), 3.79 (s, 3H), 3.99 (t, J = 7.3 Hz, 2H), 7.15–7.17 (m, 2H), 7.57 (d, J = 8.9 Hz, 1H), 7.93 (dd, J = 8.9, 2.2 Hz, 1H), 8.29 (s, 1H), 8.50 (d, J = 2.2 Hz, 1H), 9.42 ppm (s, 1H); ^{13}C NMR (CDCl_3): δ = 13.1, 19.2, 31.7, 36.0, 49.5, 113.1, 115.2, 115.2, 121.8, 123.1, 136.5, 140.4, 143.0, 149.2, 154.7 ppm; elemental analysis calcd (%) for $\text{C}_{15}\text{H}_{21}\text{N}_5\text{O}_3$: C 56.41, H 6.63, N 21.93; found: C 56.42, H 6.62, N 21.89.

Tetrabutylammonium 5-nitrobenzotriazole (7a) monohydrate: Microcrystals from acetone (96%), m.p. 91–93°C (DSC 2nd cycle m.p. 60°C); ^1H NMR (CDCl_3): δ = 0.92 (t, J = 7.2 Hz, 12H), 1.32 (sextet, J = 7.2 Hz, 8H), 1.43–1.53 (m, 8H), 3.03–3.09 (m, 8H), 7.82 (d, J = 8.9 Hz, 1H), 7.94 (dd, J = 8.9, 2.1 Hz, 1H), 8.80 ppm (d, J = 2.1 Hz, 1H); ^{13}C NMR (CDCl_3): δ = 13.4, 19.4, 23.6, 58.4, 114.3, 115.7, 116.0, 141.7, 144.1, 148.3 ppm; elemental analysis calcd (%) for $\text{C}_{22}\text{H}_{41}\text{N}_5\text{O}_3$: C 62.38, H 9.76, N 16.53; found: C 61.97, H 10.04, N 15.98.

Tetrabutylammonium 5-nitrobenzimidazole (7b): Microcrystals from acetone (99%), m.p. 99–101°C (DSC 2nd cycle m.p. 81°C); ^1H NMR (CDCl_3): δ = 0.94 (t, J = 7.0 Hz, 12H), 1.22–1.40 (m, 16H), 2.75–2.80 (m, 8H), 7.53 (d, J = 8.8 Hz, 1H), 7.89 (dd, J = 8.8, 2.3 Hz, 1H), 8.21 (s, 1H), 8.51 ppm (d, J = 2.3 Hz, 1H); ^{13}C NMR (CDCl_3): δ = 13.5, 19.4, 23.5, 58.2, 113.6, 114.2, 115.5, 139.4, 144.9, 152.0, 158.4 ppm; elemental analysis calcd (%) for $\text{C}_{23}\text{H}_{40}\text{N}_4\text{O}_2$: C 68.28, H 9.96, N 13.85; found: C 67.17, H 10.42, N 13.35.

Tetraethylammonium 5-nitrobenzotriazole (8a): Colorless oil (98%); DSC 2nd cycle m.p. 64°C; ^1H NMR (CDCl_3): δ = 1.15 (dt, J = 7.3, 1.7 Hz, 12H), 3.08 (q, J = 7.3 Hz, 8H), 7.81 (d, J = 9.0 Hz, 1H), 7.93 (dd, J = 9.0, 2.1 Hz, 1H), 8.78 ppm (d, J = 2.1 Hz, 1H); ^{13}C NMR (CDCl_3): δ = 7.3, 52.2 (t, J = 3.0 Hz, 4C), 114.1, 115.7, 116.0, 141.7, 144.2, 148.4 ppm; elemental analysis calcd (%) for $\text{C}_{14}\text{H}_{23}\text{N}_5\text{O}_2$: C 57.32, H 7.90, N 23.87; found: C 56.01, H 8.17, N 22.58.

Tetraethylammonium 5-nitrobenzimidazole (8b) monohydrate: Microcrystals from acetone (99%), m.p. 42–43°C (DSC 2nd cycle m.p. 101°C); ^1H NMR (CDCl_3): δ = 1.11 (tt, J = 7.3, 1.6 Hz, 12H), 2.97 (q, J = 7.3 Hz, 8H), 7.59 (d, J = 8.8 Hz, 1H), 7.94 (dd, J = 8.8, 2.3 Hz, 1H), 8.28 (s, 1H), 8.53 ppm (d, J = 2.2 Hz, 1H); ^{13}C NMR (CDCl_3): δ = 7.12, 52.1 (t, J = 2.9 Hz, 4C), 113.1, 115.0, 115.2, 140.3, 143.2, 149.4, 155.1 ppm; elemental analysis calcd (%) for $\text{C}_{15}\text{H}_{26}\text{N}_4\text{O}_3$: C 58.04, H 8.44, N 18.05; found: C 58.80, H 8.47, N 17.88.

Tetramethylammonium 5-nitrobenzotriazole (9a): Microcrystals from acetone (89%), m.p. 192–195°C (DSC m.p. at T_{decomp} 192°C); ^1H NMR ($[\text{D}_6]\text{DMSO}$): δ = 3.13 (s, 12H), 7.74 (d, J = 8.8 Hz, 1H), 7.82 (dd, J = 8.8, 2.1 Hz, 1H), 8.62 ppm (d, J = 2.1 Hz, 1H); ^{13}C NMR ($[\text{D}_6]\text{DMSO}$): δ = 54.3 (t, J = 4.4 Hz, 4C), 113.5, 114.6, 115.8, 140.5, 144.1, 148.4 ppm; elemental analysis calcd (%) for $\text{C}_{10}\text{H}_{15}\text{N}_5\text{O}_2$: C 50.62, H 6.37, N 29.52; found: C 50.29, H 6.73, N 28.46.

Tetramethylammonium 5-nitrobenzimidazole (9b) monohydrate: Microcrystals from acetone (93%), m.p. 66–68°C (DSC 2nd cycle m.p. 119°C); ^1H NMR ($[\text{D}_6]\text{DMSO}$): δ = 3.10 (s, 12H), 7.37 (d, J = 8.8 Hz, 1H), 7.73 (dd, J = 8.8, 2.3 Hz, 1H), 7.98 (s, 1H), 8.27 ppm (d, J = 2.3 Hz,

1H); ^{13}C NMR ($[\text{D}_6]\text{DMSO}$): δ = 54.4, 112.5, 113.0, 115.0, 137.9, 145.4, 152.9, 158.8 ppm; elemental analysis calcd (%) for $\text{C}_{11}\text{H}_{18}\text{N}_4\text{O}_3$: C 51.96, H 7.13, N 22.03; found: C 53.54, H 6.45, N 21.06.

Analyses: Melting points were determined by differential scanning calorimetry (DSC) TA Instruments model 2920 Modulated DSC (New Castle, DE) cooled with a liquid nitrogen cryostat. The calorimeter was calibrated for temperature and cell constants using indium (m.p. 156.61°C, ΔH = 28.71 J g $^{-1}$). Data were collected at constant atmospheric pressure, using samples between 10–40 mg in aluminum sample pans. Experiments were performed with heating at a rate of 5°C min $^{-1}$. The DSC instrument was adjusted so that zero heat flow was between 0 and -0.5 mW, and the baseline drift was less than 0.1 mW over the temperature range 0–180°C. An empty sample pan was used as reference.

Thermal decomposition temperatures were measured in the dynamic heating regime using a TGA 2950 TA Instrument under dried air atmosphere. Samples between 5–15 mg were heated from 40–800°C with isocratic heating rate at 5°C min $^{-1}$ under air atmosphere. Decomposition temperatures ($T_{5\% \text{ decomp}}$) were determined from both i) the onset to 5 wt% mass loss in an isocratic TGA experiment, which provides a more realistic representation of thermal stability at elevated temperatures, and ii) from the onset to complete decomposition.

X-ray crystallographic studies: Samples were recrystallized in dry ethanol by slow vapor diffusion of diethyl ether at 23°C. Single crystals suitable for X-ray analysis were isolated in air or polyfluorinated oil, mounted on fibers, and transferred to the goniometer. The crystals were cooled to -100°C with a stream of nitrogen gas and data were collected on a Siemens SMART diffractometer equipped with a CCD area detector, using graphite monochromated MoK_α radiation. The SHELXTL software (version 5) was used for each solution and refinement.^[75] Absorption corrections were made with SADABS.^[76] Each structure was refined by using full-matrix least-squares methods on F^2 .

All atoms were readily located and the positions of all non-hydrogen atoms were refined anisotropically. In a few cases disorder or possible twinning was observed. In **3i**, the one ring atom position was disordered such that it needed to be properly refined as one half C and one half N. Compound **5c** showed signs of twinning; however, PLATON could not provide a suitable twin law for successful refinement using the TWIN command. The structure for **7b-0.5H₂O** was found to have rotational disorder in the cation alkyl chain. An alternate position for this alkyl group was found and refined appropriately.

The hydrogen atoms were added in approximated positions and allowed to refine unconstrained in order to obtain proper close-contact interactions, with a few exceptions. Because of the disorder in **3i**, a hydrogen atom was added with fixed thermal parameters in a calculated position on the tetrazolate ring. Hydrogen atoms were fixed in appropriate positions for the disorder in **7b-0.5H₂O** with fixed thermal parameters.

CCDC 733814, 733815, 733816, 733817, 733818, 733819, 733820, 733821, 733822, 733823, 733824, 733825, 733826, 733827, 733828, 733829, 733830, 733831, and 733832 contain the supplementary crystallographic data for this paper. These data can be obtained free of charge from The Cambridge Crystallographic Data Centre via www.ccdc.cam.ac.uk/data_request/cif

Acknowledgements

This research was supported by the Air Force Office of Scientific Research (Grant F49620-03-1-0357).

- [1] R. D. Rogers, G. A. Voth, *Acc. Chem. Res.* **2007**, *40*, 1077–1078.
- [2] T. Welton, *Chem. Rev.* **1999**, *99*, 2071–2083.
- [3] J. D. Holbrey, K. R. Seddon, *Clean Prod. Proc.* **1999**, *1*, 223–236.
- [4] P. Wasserscheid, W. Keim, *Angew. Chem.* **2000**, *112*, 3926–3945; *Angew. Chem. Int. Ed.* **2000**, *39*, 3772–3789.
- [5] R. Sheldon, *Chem. Commun.* **2001**, 2399–2407.
- [6] C. M. Gordon, *Appl. Catal. A* **2001**, *222*, 101–117.

- [7] J. Dupont, R. F. de Souza, P. A. Z. Suarez, *Chem. Rev.* **2002**, *102*, 3667–3691.
- [8] M. T. Carter, C. L. Hussey, S. K. D. Strubinger, R. A. Osteryoung, *Inorg. Chem.* **1991**, *30*, 1149–1151.
- [9] F. Endres, *ChemPhysChem* **2002**, *3*, 144–154.
- [10] M. Gorlov, L. Kloos, *Dalton Trans.* **2008**, 2655–2666.
- [11] T. Mizumo, H. Ohno, *Yoyuen oyobi Koon Kagaku* **2007**, *50*, 5–11.
- [12] A. Fericola, B. Scrosati, H. Ohno, *Ionics* **2006**, *12*, 95–102.
- [13] A. E. Visser, R. P. Swatloski, W. M. Reichert, S. T. Griffin, R. D. Rogers, *Ind. Eng. Chem. Res.* **2000**, *39*, 3596–3604.
- [14] A. E. Visser, R. P. Swatloski, W. M. Reichert, R. Mayton, S. Sheff, A. Wierzbicki, J. H. Davis, Jr., R. D. Rogers, *Chem. Commun.* **2001**, 135–136.
- [15] S. Dai, Y. H. Ju, C. E. Barnes, *J. Chem. Soc. Dalton Trans.* **1999**, 1201–1202.
- [16] P. Wasserscheid, A. Boesmann, A. Jess, L. Datsevitch, C. Schmitz and A. Lauter, PCT Int. Appl., 2003037835, **2003**; [*Chem. Abstr.* **2003**, *138*, 370660].
- [17] X. Han, D. W. Armstrong, *Acc. Chem. Res.* **2007**, *40*, 1079–1086.
- [18] A. Berthod, M. J. Ruiz-Angel, S. Carda-Broch, *J. Chromatogr. A* **2008**, *1184*, 6–18.
- [19] C. Chiappe, D. Pieraccini, *ARKIVOC* **2002**, *11*, 249–255.
- [20] L. Kiss, T. Kurtán, S. Antus, Henri Brunner, *ARKIVOC* **2003**, *5*, 69–76.
- [21] T. Welton, *Coord. Chem. Rev.* **2004**, *248*, 2459–2477.
- [22] J. Mo, L. Xu, J. Xiao, *J. Am. Chem. Soc.* **2005**, *127*, 751–760.
- [23] J. Ding, V. Desikan, X. Han, T. L. Xiao, R. Ding, W. S. Jenks, D. W. Armstrong, *Org. Lett.* **2005**, *7*, 335–337.
- [24] P. J. Dyson, T. J. Geldbach, *Electrochem. Soc. Interface* **2007**, *16*, 50–53.
- [25] P. Wasserscheid, P. Schulz, in *Ionic Liquids in Synthesis*, 2nd ed. (Eds.: P. Wasserscheid, T. Welton), Wiley-VCH, Weinheim, **2008**, pp. 369–463.
- [26] V. I. Pârvulescu, C. Hardacre, *Chem. Rev.* **2007**, *107*, 615–2665.
- [27] S. A. Forsyth, J. M. Pringle, D. R. MacFarlane, *Aust. J. Chem.* **2004**, *57*, 113–119.
- [28] H. Ohno, in *Electrodeposition from Ionic Liquids* (Eds.: F. Endres, D. R. MacFarlane, A. P. Abbott), Wiley-VCH, Weinheim, **2008**, pp. 47–82.
- [29] N. V. Plechkova, K. R. Seddon, *Chem. Soc. Rev.* **2008**, *37*, 123–150.
- [30] C. A. Angell, N. Byrne, J.-P. Belieres, *Acc. Chem. Res.* **2007**, *40*, 1228–1236.
- [31] R. P. Swatloski, S. K. Spear, J. D. Holbrey, R. D. Rogers, *J. Am. Chem. Soc.* **2002**, *124*, 4974–4975.
- [32] H. Saitoh, *Kagaku Kagaku* **2006**, *70*, 121–127.
- [33] D. Kuang, S. Ito, B. Wenger, C. Klein, J.-E. Moser, R. Humphry-Baker, S. M. Zakeeruddin, M. Grätzel, *J. Am. Chem. Soc.* **2006**, *128*, 4146–4154.
- [34] Q. Lu, H. Wang, C. Ye, W. Liu, Q. Xue, *Tribol. Int.* **2004**, *37*, 547–552.
- [35] Z. Mu, W. Liu, S. Zhang, F. Zhou, *Chem. Lett.* **2004**, *33*, 524–525.
- [36] C. Ye, W. Liu, Y. Chen, L. Yu, *Chem. Commun.* **2001**, 2244–2245.
- [37] M. E. Van Valkenburg, R. L. Vaughn, M. Williams, J. S. Wilkes, *Thermochim. Acta* **2005**, *425*, 181–188.
- [38] J. D. Holbrey, W. M. Reichert, R. G. Reddy, R. D. Rogers in *856 ACS Symposium Series: Ionic Liquids as Green Solvents* (Eds.: R. D. Rogers, K. R. Seddon), ACS, Washington **2003**, pp. 121–133.
- [39] A. E. Jimenez, M. D. Bermudez, P. Iglesias, F. J. Carrion, G. Martinez-Nicolas, *Wear* **2006**, *260*, 766–782.
- [40] H. Kamimura, I. Minami, S. Mori, *Toraiborojitsuto* **2005**, *50*, 208–213.
- [41] G. W. Drake, T. W. Hawkins, A. Brand, L. Hall, M. McKay, A. Vij, I. Ismail, *Propellants Explos. Pyrotech.* **2003**, *28*, 174–180.
- [42] R. P. Singh, R. D. Verma, D. T. Meshri, J. M. Shreeve, *Angew. Chem.* **2006**, *118*, 3664–3682; *Angew. Chem. Int. Ed.* **2006**, *45*, 3584–3601.
- [43] A. R. Katritzky, S. Singh, K. Kirichenko, J. D. Holbrey, M. Smiglak, W. M. Reichert, R. D. Rogers, *Chem. Commun.* **2005**, 868–871.
- [44] M. Smiglak, A. Metlen, R. D. Rogers, *Acc. Chem. Res.* **2007**, *40*, 1182–1192.
- [45] S. D. Chambreau, S. Schneider, M. Rosander, T. Hawkins, C. J. Gallegos, M. F. Pastewait, G. L. Vaghjiani, *J. Phys. Chem. A* **2008**, *112*, 7816–7824.
- [46] C. B. Jones, R. Haiges, T. Schroer, K. O. Christe, *Angew. Chem.* **2006**, *118*, 5103–5106; *Angew. Chem. Int. Ed.* **2006**, *45*, 4981–4984.
- [47] T. M. Klapötke, P. Mayer, A. Schulz, J. J. Weigand, *J. Am. Chem. Soc.* **2005**, *127*, 2032–2033.
- [48] T. M. Klapötke, G. Holl, *Green Chem.* **2001**, *3*, G75–G77.
- [49] H. Bircher, *Chimia* **2004**, *58*, 355–362.
- [50] R. Meyer, J. Köhler, A. Homburg, *Explosives*, 5th ed., Wiley-VCH, Weinheim, **2002**.
- [51] A. Bailey, S. G. Murray in *Explosives Propellants and Pyrotechnics*, Brasey's, London, **1989**.
- [52] H.-J. Laas, R. Halpaap, F. Richter, J. Kocher, US Patent 20030204041, **2003**.
- [53] M. Stearcey, P. L. Pye, J. B. Lee, *Synth. Commun.* **1989**, *19*, 1309–1315.
- [54] W. Ogiwara, M. Yoshizawa, H. Ohno, *Chem. Lett.* **2004**, *33*, 1022–1023.
- [55] H. Ohno, M. Yoshizawa, W. Ogiwara, H. Ogawa, H. Taguchi, Jpn. Patent 2004331521, **2004**.
- [56] H. Xue, Y. Gao, B. Twamley, J. M. Shreeve, *Inorg. Chem.* **2005**, *44*, 5068–5072.
- [57] C. F. Ye, J. C. Xiao, B. Twamley, J. M. Shreeve, *Chem. Commun.* **2005**, 2750–2752.
- [58] H. Xue, B. Twamley, J. M. Shreeve, *J. Mater. Chem.* **2005**, *15*, 3459–3465.
- [59] G.-H. Tao, Y. Guo, Y.-H. Joo, B. Twamley, J. M. Shreeve, *J. Mater. Chem.* **2008**, *18*, 5524–5530.
- [60] C. L. Liotta, P. Pollet, M. A. Belcher, J. B. Aronson, S. Samanta, K. N. Griffith, US Patent 20050269001A1, **2005**.
- [61] T. M. Klapötke, C. M. Sabaté, J. M. Welch, *Dalton Trans.* **2008**, 6372–6380.
- [62] A. R. Katritzky, S. Singh, K. Kirichenko, M. Smiglak, J. D. Holbrey, W. M. Reichert, S. K. Spear, R. D. Rogers, *Chem. Eur. J.* **2006**, *12*, 4630–4641.
- [63] A. Hammerl, M. A. Hiskey, G. Holl, T. M. Klapötke, K. Polborn, R. Stierstorfer, J. J. Weigand, *Chem. Mater.* **2005**, *17*, 3784–3793.
- [64] A. Hammerl, G. Holl, T. M. Klapötke, P. Mayer, H. Noth, H. Piotrowski, M. Warchhold, *Eur. J. Inorg. Chem.* **2002**, 834–845.
- [65] K. Y. Lee, D. G. Ott, M. M. Stinecipher, *Ind. Eng. Chem. Proc. Res. Dev.* **1981**, *20*, 358–360.
- [66] K. Y. Lee, D. G. Ott, US Patent US4236014, **1979**.
- [67] J. D. Holbrey, W. M. Reichert, R. P. Swatloski, G. A. Broker, W. R. Pitner, K. R. Seddon, R. D. Rogers, *Green Chem.* **2002**, *4*, 407–413.
- [68] W. Xie, R. Xie, W.-P. Pan, D. Hunter, B. Koene, L.-S. Tan, V. R. Loon-Seng, *Chem. Mater.* **2002**, *14*, 4837–4845.
- [69] K. W. Habiger, J. R. Clifford, R. B. Miller, W. F. McCullough, *Conf. Rec. Proc. IEEE Part. Accel. Conf.* **1994**, *4*, 2622–2624.
- [70] V. M. Chernyshev, N. D. Zemlyakov, V. B. Il'in, V. A. Taranushich, *Russ. J. Appl. Chem.* **2000**, *73*, 839–841; V. M. Chernyshev, N. D. Zemlyakov, V. B. Il'in, V. A. Taranushich, *Zh. Prikl. Khim.* **2000**, *73*, 791–793.
- [71] T. E. Eagles, M. A. Khan, B. M. Lynch, *Org. Prep. Proced. Int.* **1970**, *2*, 117–119.
- [72] S. Bulusu, R. Damavarapu, J. R. Autera, R. Behrens, Jr., L. M. Minier, J. Villanueva, K. Jayasuriya, T. Axenrod, *J. Phys. Chem.* **1995**, *99*, 5009–5015.
- [73] S. S. Novikov, L. I. Khmel'nitskii, O. V. Lebedev, V. V. Sevast'yanova, L. V. Epishina, *Chem. Heterocycl. Compd.* **1970**, *6*, 465–469.
- [74] M. R. Grimmett, S.-T. Hua, K.-C. Chang, S. A. Foley, J. Simpson, *Aust. J. Chem.* **1989**, *42*, 1281–1289.
- [75] SHELXTL, Version 5.05, G. M. Sheldrick, Seimens Analytical X-ray Instruments Inc., **1996**.
- [76] Program for Semiempirical Absorption Correction of Area Detector Data, G. M. Sheldrick, University of Göttingen, Göttingen, **1996**.

Received: May 27, 2009
Published online: December 28, 2009